one set of solutions satisfies the entire data and a new solution, including these results, is required.

ACKNOWLEDGMENTS

This experiment could not have been completed without the active support of many members of the staff of the Rutherford Laboratory. We especially wish to thank D. A. Gray and his colleagues for the successful operation of Nimrod and H. H. Atkinson and his colleagues for the construction and assistance in the operation of the polarized proton target.

We are indebted to P. J. Coleman, R. Downton, D. A. Morris, J. E. Rivers-Moore, and D. C. Thomas for their able assistance in setting up the experiment and taking data.

The electronic logic units used in this work were designed by J. V. Cresswell and P. Wilde, and the interface with the PDP-5 was constructed by W. M. Evans. We are most grateful to them and their colleagues for their constant help and advice.

Three of us (C. R. C., K. S. H., and J. C. S.) wish to acknowledge the receipt of maintenance grants from the Science Research Council during this experiment.

PHYSICAL REVIEW VOLUME 184, NUMBER 5 25 AUGUST 1969

Investigation of the Final States $K^-\pi^-\pi^+\pi^0 p$ and $K^-\pi^-\pi^+\pi^+ n$ Produced in K^-p Interactions at 4.6 and 5.0 BeV/c*

R. E. JUHALA,† R. A. LEACOCK, AND J. I. RHODE
Institute for Atomic Research and Department of Physics, Iowa State University, Ames, Iowa 50010

AND

J. B. KOPELMAN, L. MARSHALL LIBBY, AND E. URVATER‡
Department of Physics, University of Colorado, Boulder, Colorado 80302

(Received 10 October 1968)

We have studied the reactions $K^-p \to K^-\pi^-\pi^+\pi^0 p$ and $K^-p \to K^-\pi^-\pi^+\pi^+ n$ at 4.6- and 5.0-BeV/c incident K^- momenta. Production cross sections for the $K^-\pi^-\pi^-\pi^+\pi^0 p$ state are 0.76±0.09 and 0.93±0.12 mb, and for the $K^-\pi^-\pi^+\pi^+ n$ state 0.42±0.06 and 0.39±0.07 mb, at 4.6 and 5.0 BeV/c, respectively. The combined sample for the $K^-\pi^-\pi^+\pi^0 p$ state contains 1305 events. Resonance contributions include: $\bar{K}^{*0}(890)$, (19±3)%; $K^{*-}(890)$, (7.2±1.7)%; $\Delta^{++}(1236)$, (14.5±2.5)%; $\Delta^+(1236)$, (8±3)%; $\Delta^0(1236)$, <2%; $\omega^0(784)$, (14.5±3)%; $\eta(548)$, (3.3±1.3)%; a 1060-MeV 3π effect identified as the $A_1{}^0(1080)$, (10.5±3)%; $A_2{}^0(1300)$, (3±1.5)%; $\rho^+(760)$, (9±2.5)%; $\rho^-(760)$, (5.5±2)%; and a ~960-MeV narrow 3π enhancement, (2.5±1)%. The $A_1{}^0$ is produced in this reaction in a way precluding contributions from the Deck effect. A spin-parity analysis for the $A_1{}^0$ provides good evidence that the spin-parity is in the sequence 0^-, 1^+, 2^-, ... Our results are consistent with the previously favored 1^+ assignment. We have 701 events in the combined sample for the $K^-\pi^-\pi^+\pi^+ n$ final state. Contributions to this channel from accepted or suspected resonance states include: $\bar{K}^{*0}(890)$, (29±4)%; $\Delta^-(1236)$, (17±3)%; $\Delta^+(1236)$, (7±2)%; and a narrow 960-MeV $\pi^+\pi^+\pi^-$ effect, (6±2)%. Addition of $K^*\pi$ and $K\rho$ distributions from both final states corresponding to specific values of I_3 provides good evidence for production of $K_A(1320)$ and $K_N(1420)$. A similar treatment of $I_3=\frac{3}{2}$ $\Delta(1236)\pi$ and $N\rho(760)$ distributions indicates an effect near 1820 MeV.

I. INTRODUCTION

WE here present results of an investigation of the following five-body final states observed in K^-p interactions at 4.6 and 5.0 BeV/c:

$$K^-\pi^-\pi^+\pi^0 p, \quad (1)$$

$$K^-\pi^-\pi^+\pi^+ n. \quad (2)$$

This paper deals only with the combined data from both momenta. No general investigations of these final states (at 4.6–5.0-BeV/c K^- momenta) have appeared in the literature. Certain aspects of reaction (1) at 3.8 BeV/c have been published previously.[1,2] Also, an analysis of these reactions at 4.1 BeV/c and, particularly, at 5.5 BeV/c is currently being undertaken by another group.[3]

In the present paper we provide a comprehensive review of our investigations of these reactions. In Sec. II we present pertinent details of our analysis procedures. Additional information on background estimates and on weighted phase space is given in Ap-

* Work performed in Ames Laboratory of U. S. Atomic Energy Commission. Contribution No. 2365.

† Present address: National Accelerator Laboratory, P.O. Box 500, Batavia, Ill. 60510.

‡ Present address: Dept. of Physics, City College of CUNY, New York, N. Y. 10031.

[1] D. D. Carmony, T. Hendricks, and R. L. Lander, Phys. Rev. Letters **18**, 615 (1967).

[2] J. Field, T. Hendricks, O. Piccioni, and P. Yager, Phys. Letters **24B**, 638 (1967).

[3] G. Chandler (private communication).

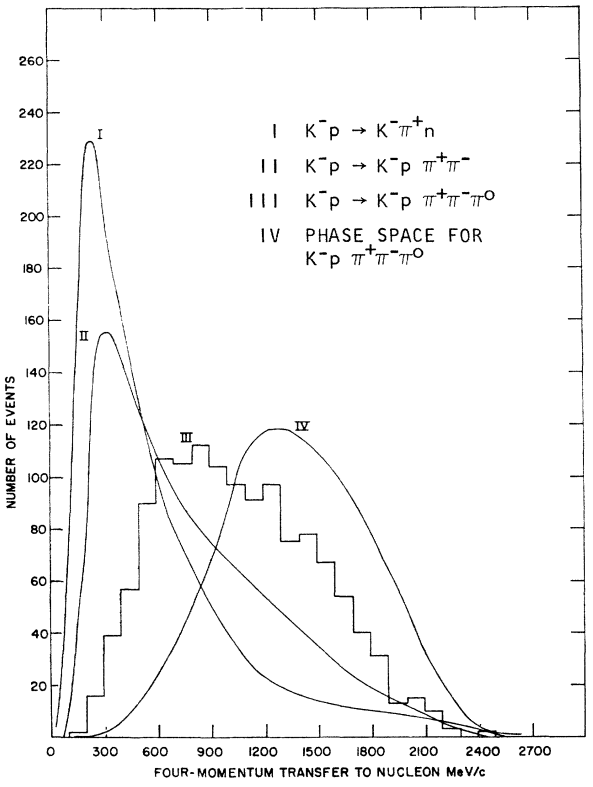

FIG. 1. Distributions in four-momentum transfer between target and final-state nucleon for three-, four-, and five-body final states produced in K^-p interactions at 4.6 and 5.0 BeV/c.

pendices A and B. In Secs. III and IV specific features of the two reactions are considered. Cross sections for resonance production are presented, and various gross and selected mass distributions are considered. Production characteristics of important resonances are presented and discussed. In connection with consideration of the $\pi^+\pi^-\pi^0$ channel for reaction (1), we provide additional information on A_1^0 production. In Sec. V special combinations of $K\pi\pi$ spectra from both reactions (1) and (2) are presented in a search for higher K^*'s. Evidence is found for production of $K_A(1320)$ and $K_N(1420)$. A parallel analysis of $N\pi\pi$ distributions is given in Sec. VI. An enhancement near 1820 MeV in the $I_3=\frac{3}{2}$ $N\pi\pi$ system is noted. Discussion and interpretation of various features of the data are included in Sec. VII.

TABLE I. Event summary.

	Beam momentum		
	4.6 BeV/c	5.0 BeV/c	Combined
No. of frames	26 200	25 500	51 700
Eff. K^- track length (10^7 cm)	4.1	2.5	6.6
No. of meas. four-prongs	10 750	5 500	16 250
Fits to $K^-\pi^-\pi^+\pi^0 p$	743	562	1305
$\sigma(K^-\pi^-\pi^+\pi^0 p)$[a] (mb)	0.76±0.09	0.93±0.12	0.83±0.12
Fits to $K^-\pi^-\pi^+\pi^+ n$	419	282	701
$\sigma(K^-\pi^-\pi^+\pi^+ n)$[a] (mb)	0.42±0.06	0.39±0.07	0.41±0.07

[a] Cross sections presented here are derived from indicated K^- track lengths and numbers of fits, with additional correction factors.

II. EXPERIMENTAL RESULTS

Approximately 16 000 measured four-prong events from 52 000 frames of K^-p interactions in the Brookhaven National Laboratory 80-in. bubble chamber were processed to obtain event samples of 1305 and 701 events, respectively, for reactions (1) and (2). Pertinent details of the exposure and analysis are presented in Table I in a breakdown by beam momentum. Kinematic fits to all constrained final states were tried.[4] Restrictions on missing mass and beam parameters have been imposed.[5] The relative contamination in each sample is estimated to be less than 22% and consists in each case of a number of small contributions from various sources (see Appendix A).

Cross sections are determined on the basis of a triple scan (for all interactions) of about half the film at each beam momentum. The effective K^- track length for these subsets of the complete exposure is calculated with the following input information: a beam-track count for every fifth frame, a δ-ray scan, and the number of observed τ decays. Our determinations of total K^-p cross sections are in good agreement with values obtained at these momenta by other workers.[6]

The analysis procedures followed in this study are for the most part conventional. In investigating effective-mass distributions, however, we have made considerable use of what we refer to as weighted-phase-space comparison curves. This is an approximate method of correcting the background in any specific channel for the reflection (in that channel) of resonance effects in other channels. It involves, specifically, assigning to each event of a set of Monte-Carlo-generated phase-space events a weight which is the ratio of the experimentally observed number of events per unit mass interval for the particular channel to be weighted on to the corresponding number determined for the usual unweighted phase space. In forming the weighted invariant-mass distribution for any given channel, a histogram of the accumulated weights rather than events is produced. This weighting procedure satisfies

[4] Events included in each of these samples were required to have an ionization-consistent fit to the reaction hypothesis in question with $\chi^2 \leq 5$. A 5:1 χ^2-probability ratio was used where applicable to choose among multiple fits satisfying the above criterion. By this we mean that no fit to the reaction hypotheses of interest was used if the χ^2 probability (i.e., the probability of obtaining a larger χ^2) for some other hypotheses was more than five times as great. Events which remained ambiguous under these procedures were distributed among contending hypotheses for which fits were obtained on a straight χ^2-probability basis. No event is assigned to more than a single final state and each event is counted only once in a given sample.

[5] The beam track of each event in the final selected samples is required to have dip angle within a specified range and azimuth angle within limits which are expressed as functions of the position of the event vertex in the beam direction.

[6] A. Fridman and A. Michalon, Nuovo Cimento 68, 344 (1967).

TABLE II. Results of fits[a] to gross-mass spectra for reactions (1) and (2).

Final state	Channel	Resonance	Experimental mass (MeV)	Corrected width[b] (MeV)	χ^2 probability	% contribution	Cross section (μb)
$K^-\pi^-\pi^+\pi^0 p$	$p\pi^+$	Δ^{++}	1206±20	75±20	0.52	14.5±2.5	120±22
	$p\pi^0$	Δ^+	1220±20	90±20	0.01	8.0±3.0	66±22
	$\pi^+\pi^0$	ρ^+	765±20	95±20	0.11	9.0±2.5	74±19
	$\pi^-\pi^0$	ρ^-	769±20	100±25	0.20	5.5±2.0	45±15
	$K^-\pi^+$	$\bar{K}^{*0}$	890±13	65±15	0.50	19.0±3.0	157±30
	$K^-\pi^0$	K^{*-}	879±15	60±15	0.31	7.2±1.7	59±15
	$\pi^+\pi^-\pi^0$	η	547±10	~0±10	0.90	3.3±1.3	27± 9
		ω	783±10	10±10		14.5±3.0	120±25
		"δ"	948±20	~0±10		2.5±1.0	21± 7
		A_1^0	1069±20	120±20		10.5±3.0	87±22
		A_2^0	1324±25	85±20		3.0±1.5	25±11
$K^-\pi^-\pi^+\pi^+ n$	$n\pi^+$	Δ^+	1259±20	60±20	0.60	7.0±2.0	29± 9
	$n\pi^-$	Δ^-	1225±20	100±20	0.40	17.0±3.0	70±12
	$K^-\pi^+$	$\bar{K}^{*0}$	895±12	61±15	0.40	29.0±4.0	119±20
	$\pi^+\pi^+\pi^-$	"δ"	960±15	~0±10	0.75	6.0±2.0	24± 8

[a] Resonance contributions and parameters quoted here are determined from fits to the respective mass distributions using fixed-width nonrelativistic Breit-Wigner resonance functions with appropriate weighted-phase-space backgrounds (see Appendix B). Errors are not obtained from the fits, but are determined from other considerations (see Ref. 8).

[b] In determining intrinsic resonance widths we have employed a set of curves of experimental width (full width at half-maximum) versus experimental resolution (σ in an assumed Gaussian resolution function). These are formed by Monte Carlo generation of distributions according to nonrelativistic fixed-width BW forms (for various choices of width) and subsequent smearing by a Gaussian resolution function (with various choices of σ). The full width at half-maximum of the resulting distributions is determined and plotted against σ. Our experimental mass resolution is calculated using the adjusted errors obtained from the kinematic fit by standard methods as a function of mass for each distribution of interest.

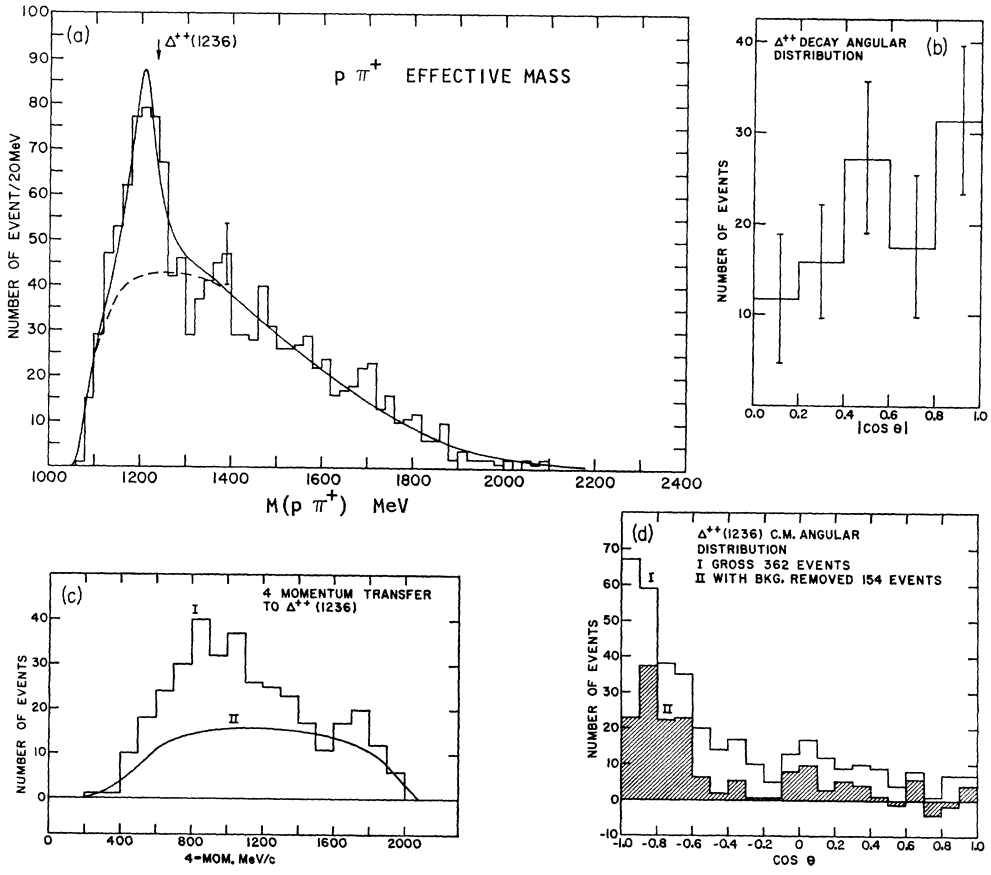

FIG. 2. Effective-mass distribution for $p\pi^+$ system from reaction (1), and angular and four-momentum-transfer distributions for Δ^{++}. In (c), I is the histogram for Δ^{++} events and II is the background shape determined from corresponding distributions for events with $p\pi^+$ mass adjacent to the Δ^{++} band. The Δ^{++} decay angular distribution (b) is for a subsample of Δ^{++} events from which $\bar{K}^{*0}$ events have been removed and for which the four-momentum transfer between the target proton and outgoing Δ^{++} system is less than 1100 MeV/c. A background correction has been applied. Angles in (b) are referred to the incident proton direction seen in the Δ^{++} rest frame.

TABLE III. Summary of miscellaneous effects[a] in channels not included in Table II.

Final state	Channel	Comments	Contributions (%)	Figure
$K^-\pi^-\pi^+\pi^0 p$	$\Delta^{++}\pi^-$	2.5–3.0-std.-dev. effects near $N^*(1525)$ and $N^*(1688)$		
	$\Delta^{++}\pi^0$	2.5-std.-dev. effect at 1850 MeV		
	$\Delta^{++}K^{*-}\pi^-$	Double-res. prod.; ~30% of K^{*-} produced with Δ^{++}	~2	
	$\Delta^{++}\pi^-\pi^0$	Only weak effects, <2 std. dev.		
	$p\pi^-$	2-std.-dev. effect in $\Delta^0(1236)$ region	~2	9(e)
	$\Delta^0\bar{K}^{*0}\pi^0$, $\Delta^0K^{*-}\pi^+$		≤1	
	$\Delta^+\pi^+$	2.5-std.-dev. effect at 1850 MeV		
	$K^-\pi^+\pi^-$ recoiling against Δ^+	~4-std.-dev. excess in 1260–1500-MeV region		
	$\Delta^+K_V(1420)$	Signal apparent		
	$\Delta^+\bar{K}^{*0}\pi^-$		~4	
	$\bar{K}^{*0}\pi^-$	Effects at 1420 and 1300 MeV		
	$\bar{K}^{*0}\pi^0$	Effects at 1420 and 1300 MeV		
	$K^{*-}p$	2-std.-dev. effect at 1900 MeV		
	$K^*\pi^+\pi^-$	Only weak effects, <2 std. dev.		
	$K^{*-}\pi^+$	2.5–3.0-std.-dev. effects at 1300 and 1400 MeV; weaker effect at 1140 MeV		
	$\pi^+\pi^-$	2.4-std.-dev. effect at 480 MeV, evidence for ρ^0	~2	9(a)
	$\rho^+\pi^-$, $\rho^-\pi^+$	Enhancement in A_1^0 region (see text)	~10	6(b)
		Enhancement in A_1^0 region (see text)		
	$\pi^+\pi^0+\pi^-\pi^0$ for A_1^0 events	Strong ρ signal	~10	6(d)
	$\pi^+\pi^-$ for A_1^0 events	No ρ^0 signal		6(c)
	ρ^+p	2.5-std.-dev. effect at 1820 MeV		
	ρ^+K^-	2.0-std.-dev. effect at 1420 and 1710 MeV		
	ω^0K	Enhancements near upper and lower ends of histogram		8(a)
	$\omega^0\rho$	2.5-std.-dev. effect at 1780 MeV		
	$K^-A_1^0$	Weak effect at ~1720 MeV		
$K^-\pi^-\pi^+\pi^+n$	$\Delta^-\bar{K}^{*0}\pi^+$		~4	
	$\Delta^+\bar{K}^{*0}\pi^-$		<3.5	
	$\Delta^+\pi^-$	~2.0-std.-dev. effect at 1820 MeV		
	$\bar{K}^{*0}\pi^-$	2–3-std.-dev. effects at 1220, 1300, and 1420 MeV		
	$\pi^+\pi^-$ for $\pi^+\pi^+\pi^-$ in A_2^0 region	Only weak evidence for ρ^0		
	$K^-\pi^-$	Effect near 900 MeV, origin unclear		18(e)
Both	$K^*\pi$ and $K\rho$ for $I_3=\pm\frac{1}{2}$	$K_A(1320)$	~3.3	21(b)
		$K_N(1420)$	~6.3	
	$\Delta\pi$ and ρp for $I_3=\frac{3}{2}$	Effect near 1840 MeV	~3.3	22(b)
	$\Delta\pi$ and ρp for $I_3=-\frac{1}{2}$	Effects at ~1880 MeV	~2.4	22(a)
		~1690 MeV	~1.0	
		~1570 MeV	~2.0	

[a] Results presented here are obtained from visual examination of pertinent mass distributions. Many channels not specifically mentioned here have been examined but indicated no structure, or less significant structure. It is not claimed that all effects noted have a physical (rather than statistical) origin; nor is it unlikely that some real physical effects contributing weakly in these or other channels have been unrecognized.

the requirement (when only a single weighting channel is used) that the distribution in weighted phase space for the same channel which is being weighted on should reproduce the experimentally observed distribution for that channel. When more than one weighting channel is used, a product of weights is formed. In this case the weighted distribution for the weighting channels will not exactly match the experimental input distribution for these channels. Additional complications arise when weighting on channels in which more than one combination per event may be formed, e.g., in weighting on $K^-\pi^+$ in the $K^-\pi^-\pi^+\pi^+n$ final state. These questions are discussed in Appendix B. The use of this technique in the analysis of a final state is appropriate only if unweighted phase space provides at least a reasonable representation of the principal features of the data. In highly peripheral interactions there are strong correlations in angles between certain final-state particles, which reflect in part the preference for production with low four-momentum transfer between target and final-state baryon and between projectile and associated final-state particles. In such cases phase space is a poor starting point for additional corrections. However, the two final states of interest in this report are much less peripheral than three- and four-body states produced in π or K interactions in this momentum range. This is illustrated in Fig. 1, which shows the distributions in four-momentum transfer ($\sqrt{-t}$) to the baryon for the $K^-\pi^-\pi^+\pi^0 p$ state considered here and for the $K^-\pi^-\pi^+p$ and $K^-\pi^+n$ final

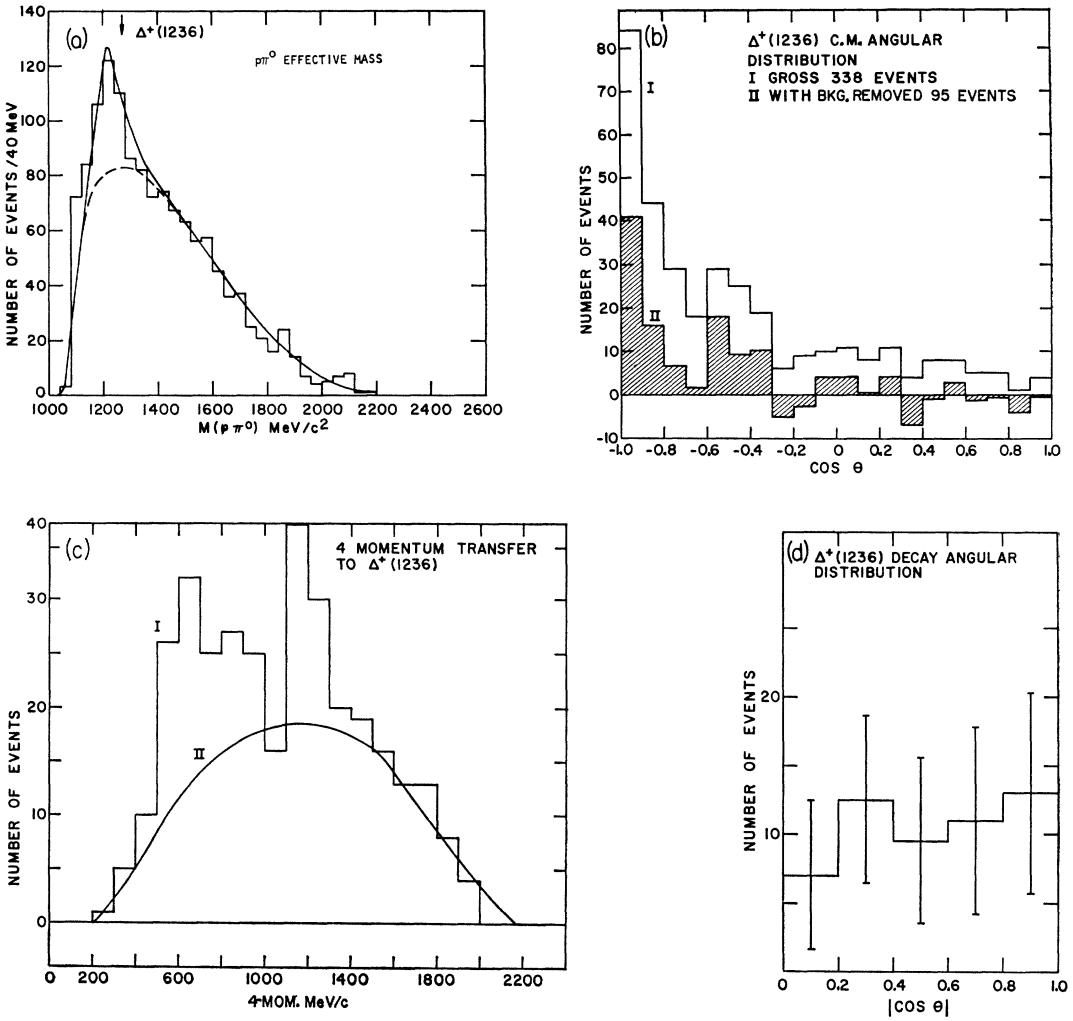

FIG. 3. Effective-mass distribution for $p\pi^0$ system from reaction (1), and angular and four-momentum-transfer distributions for Δ^+. In (c), I is the histogram for Δ^+ events and II is the background shape determined from corresponding distributions for events with $p\pi^0$ mass adjacent to the Δ^+ band. The Δ^+ decay angular distribution (d) is for a subsample of Δ^+ events from which K^{*-} events have been removed and for which the four-momentum transfer between the target proton and outgoing Δ^+ system is less than 1300 MeV/c. A background correction has been applied. Angles for (d) are referred to the incident proton direction seen in the Δ^+ rest frame.

states produced in K^-p interactions at the same momentum. In addition, the pure phase-space distribution is included for comparison. The distribution for the five-body state is less peaked at low four-momentum-transfer values than that for either the three- or four-body states; in fact, it follows phase space about as closely as it follows the four-body curve. Mass distributions for many of the channels studied in the two final states considered in this paper are well accounted for by unweighted phase space (plus additional resonance features in certain cases). In such channels there is little difference between weighted and unweighted phase space. Generally, where there is a difference between unweighted and weighted phase space, the latter provides a better representation of the distributions.

Contributions of known or suspected resonances[7] in the various effective-mass channels for the reactions considered here are determined from either maximum-likelihood or χ^2 fits, utilizing Breit-Wigner resonance functions and weighted-phase-space backgrounds (see Appendix B). Generally, resonance intensity, mass, and width are all varied in the fitting procedure, though in certain cases the mass and/or width of certain resonances are constrained. Errors in resonance contributions and parameters are not extracted formally from the fits, but instead are determined by empirical

[7] Unless otherwise indicated, parameters of resonance states are taken from N. Barash-Schmidt, A. Barbaro-Galtieri, L. R. Price, A. H. Rosenfeld, P. Soding, and C. G. Wohl, Rev. Mod. Phys. 41, 109 (1969).

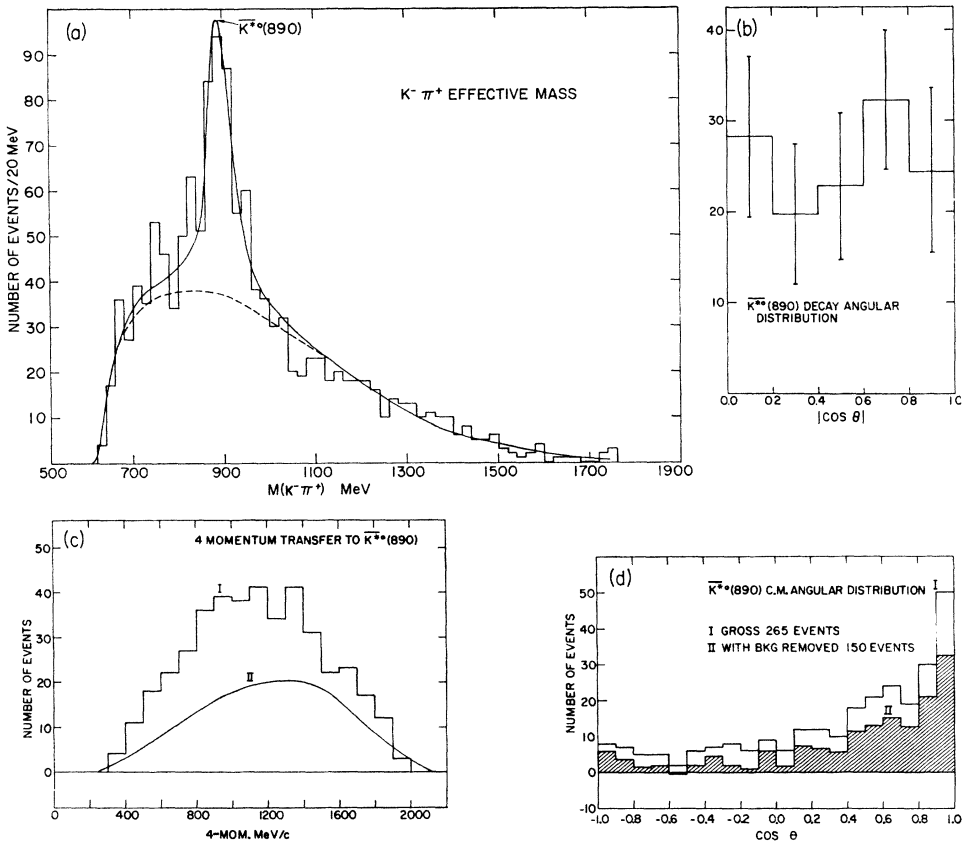

FIG. 4. Effective-mass distribution for $K^-\pi^+$ system from reaction (1) and angular and four-momentum-transfer distributions for $\bar{K}^{*0}$. In (c), I is the histogram for $\bar{K}^{*0}$ events and II is the background shape determined from corresponding distributions for events with $K^-\pi^+$ mass adjacent to the $\bar{K}^{*0}$ band. The $\bar{K}^{*0}$ decay angular distribution (b) is for a subsample of $\bar{K}^{*0}$ events from which Δ^{++} events have been removed and for which the four-momentum transfer from projectile to outgoing $K^-\pi^+$ system is less than 1400 MeV/c. A background correction has been applied. Angles in (b) are referred to the incident K^- direction seen in the $\bar{K}^{*0}$ rest frame.

procedures.[8] Such a procedure provides a useful method for parametrizing our distributions, one which is closely related to the idea of resonance production superposed on a statistical or modified statistical background. It does not specifically account for true double-resonance production in disjoint channels or for interference between resonances in intersecting channels.[9] Also, the relative orbital angular momentum of the resonating particles, which affects the shape of wide resonances, is ignored here.

[8] With regard to resonance contributions, the errors are assigned in the following manner: The number of events above a weighted-phase-space curve normalized to the total distribution is taken as a lower limit to the contribution. The error is estimated to be some fraction of the difference between the contribution determined from the fit and this lower limit. In no case is the error estimate less than the statistical uncertainty in the enhancement, which is taken to be the square root of the total number of events in the resonance band. Errors in masses and widths of resonances are estimated from a study of variations in these parameters with changes in the functional form being used in the fit (i.e., alterations in the background shape, addition of other resonance terms, removal or addition of constraints on other parameters, etc.) and other considerations.

[9] Two channels are here described as disjoint if they share no particles in common, adjoint if one is a subset of the other, and intersecting if they share one or more particles but are not adjoint.

III. $K^-\pi^-\pi^+\pi^0 p$ FINAL STATE

For this final state, 25 two-, three-, and four-body effective-mass combinations can be formed. A summary of results of our fitting procedures for these various channels is presented in Table II. Effects in channels not explicitly discussed in the text or indicated in Table II are summarized in Table III. Effective-mass distributions for the 25 channels in this final state are presented in Figs. 2–11. For the more significant enhancements we also present center-of-mass angular distributions, four-momentum-transfer distributions, and decay angular correlations. Approximate backgrounds for most of these distributions are obtained from corresponding distributions for events from mass regions immediately adjacent to the peaks considered.

A. Baryon Resonances

1. Δ^{++}

Figure 2(a) shows the $p\pi^+$ effective-mass spectrum. The 8-standard-deviation enhancement just above 1200 MeV is assumed to be the $\Delta^{++}(1236)$. The dis-

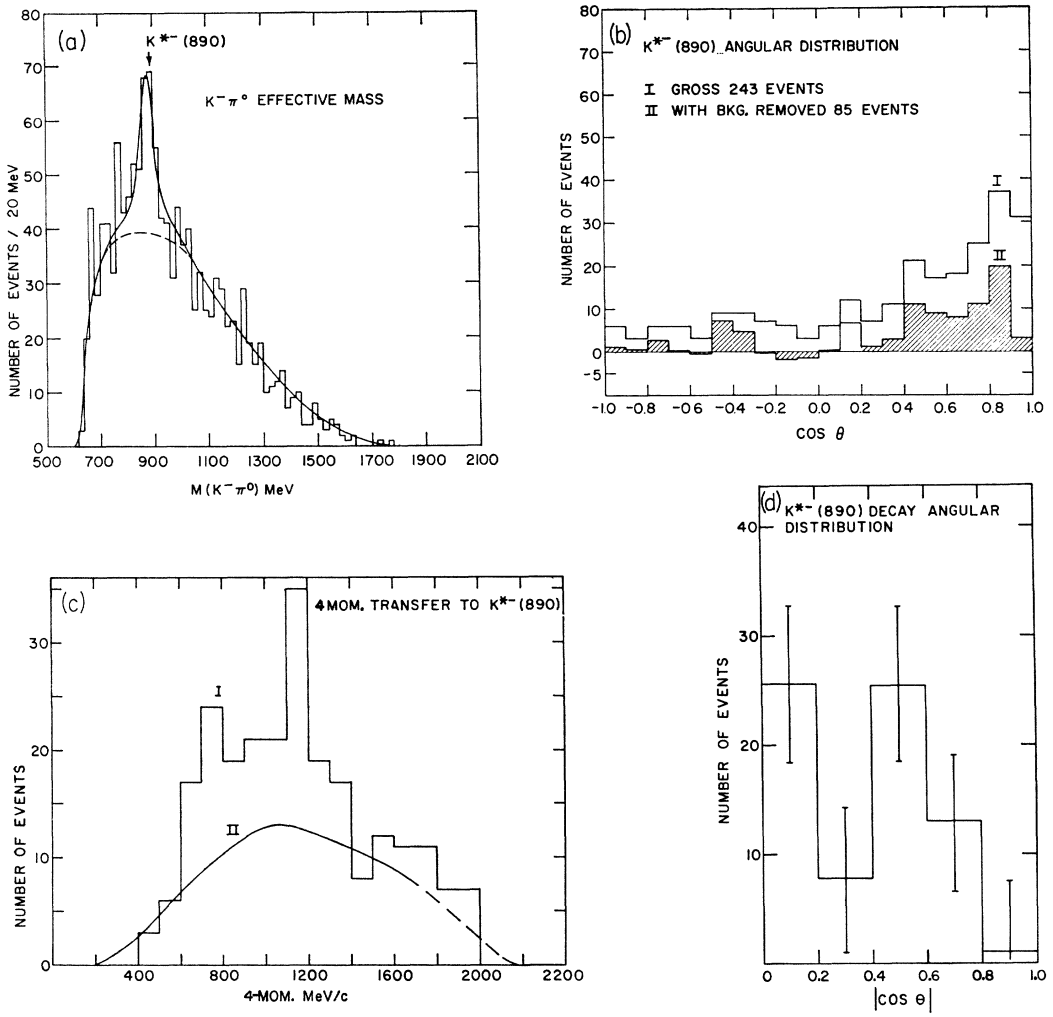

FIG. 5. Effective-mass distribution for $K^-\pi^0$ system from reaction (1) and angular and four-momentum-transfer distributions for K^{*-}. In (c), I is the histogram for K^{*-} events and II is the background shape determined from the corresponding distributions for events with $K^-\pi^0$ mass adjacent to the K^{*-} band. The K^{*-} decay angular distribution (d) is for a subsample of K^{*-} events from which Δ^+ events have been removed and for which the four-momentum transfer from projectile to outgoing $K^-\pi^0$ system is less than 1400 MeV/c. A background correction has been applied. Angles in (d) are referred to the incident K^- direction seen in the K^{*-} rest frame.

tribution is fitted with a single-resonance function plus a phase-space background weighted on the experimental $K^-\pi^+$ and $\pi^+\pi^-\pi^0$ mass distributions. (Weighted phase space peaks at a lower mass value than unweighted phase space.) Our experimentally determined mass and width for the $\Delta^{++}(1236)$ are consistent with values obtained in other experiments. The center-of-mass angular distribution for Δ^{++} events is presented in Fig. 2(d). The unshaded histogram is the distribution before background subtraction, and the shaded one is the distribution with background removed. Both distributions are backward-peaked, but the distribution with background removed is more strongly peaked than the gross distribution. In this final state the Δ^{++} is formed preferentially in processes in which the four-momentum transfer from target to outgoing $p\pi^+$ system is small. Figure 2(c) shows the four-momentum-transfer ($\sqrt{-t}$) distribution for events in the Δ^{++} region. The smooth curve indicates the background, again formed from events above and below the Δ^{++}, normalized to the estimated background contribution in the Δ^{++} region. There is an excess of events over background below 1100 MeV/c. By requiring events in the Δ^{++} region to have four-momentum transfer less than 1100 MeV/c, the background can be reduced. The decay angular distribution for low-four-momentum-transfer Δ^{++} events (also excluding $\bar{K}^{*0}$) is presented in Fig. 2(b). The decay angle is the angle between the outgoing and incoming proton, seen in the Δ^{++} rest frame. The χ^2 probability for an isotropic fit to this distribution is 0.20. There is, however, a suggestion of a $\cos^2\theta$ component. Fitting the form $a+b\cos^2\theta$ to the data yields a χ^2 probability of 0.40. This may indicate that a process such as that in

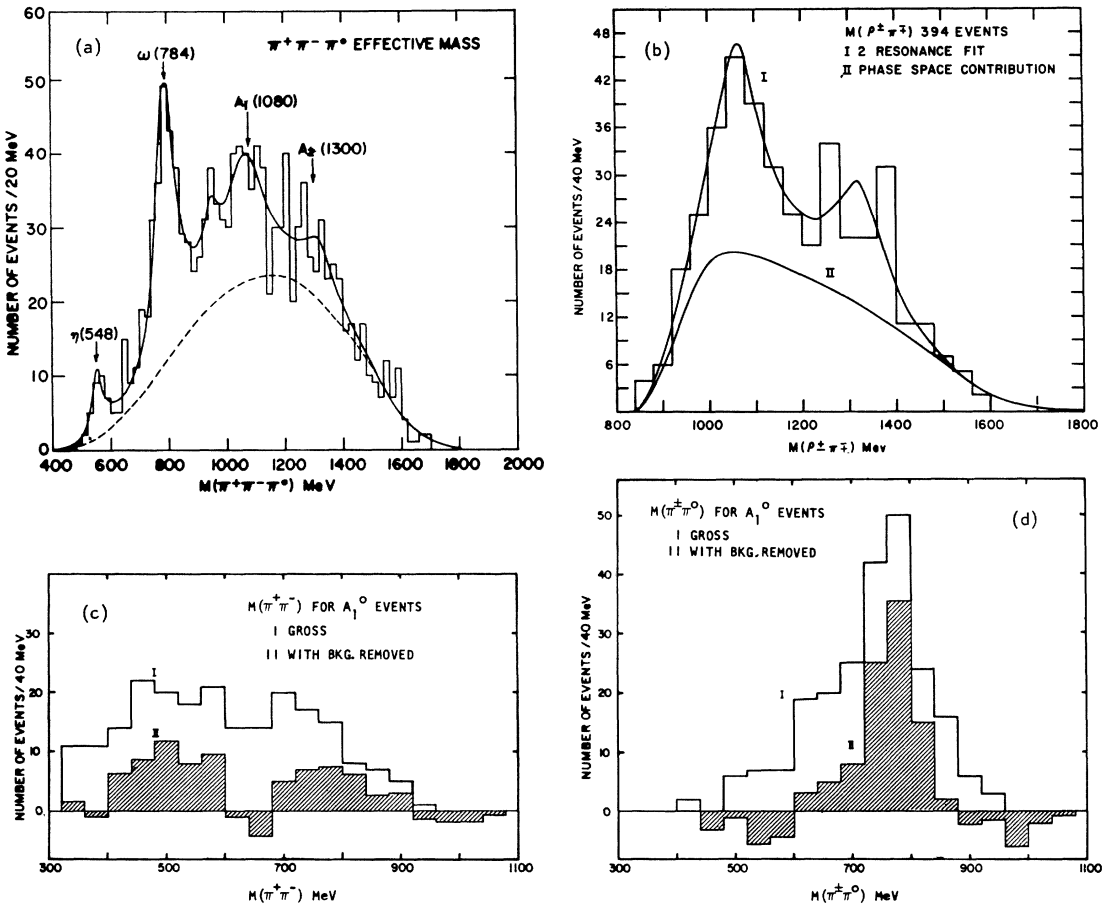

FIG. 6. Effective-mass distribution for $\pi^+\pi^-\pi^0$ system from reaction (1) and A_1^0 mass spectra. (a) Gross $\pi^+\pi^-\pi^0$ mass distribution. The solid curve is a maximum-likelihood fit using Breit-Wigner resonance functions for the η^0, ω^0, A_1^0, A_2^0, and the 960-MeV effect. The dashed curve is the weighted-phase-space contribution for this fit. (b) $\pi^+\pi^-\pi^0$ mass distribution for events with $\pi^+\pi^0$ and/or $\pi^-\pi^0$ mass in 760±60-MeV band. Curve I is a maximum-likelihood fit using Breit-Wigner resonance functions for the A_1^0 and the A_2^0. Curve II is the weighted-phase-space contribution for this fit. (c) $\pi^+\pi^-$ mass distribution for A_1^0 events. I is for all events with $\pi^+\pi^-\pi^0$ mass in A_1^0 region. II is histogram I corrected for background. (d) $\pi^\pm\pi^0$ mass distribution obtained by folding a $\pi^+\pi^0$-$\pi^-\pi^0$ mass-scatter plot along the diagonal and projecting onto the axis perpendicular to the superposed ρ bands. I is for all events with $\pi^+\pi^-\pi^0$ mass in the A_1^0 region (1060±60 MeV). II is histogram I corrected for background.

Fig. 23(f) (with the exchanged system assumed to be a π) is contributing in the production of the Δ^{++}.

2. Δ^+

The $p\pi^0$ mass distribution [Fig. 3(a)] exhibits a 4-standard-deviation enhancement near 1230 MeV, which is interpreted as the $\Delta^+(1236)$. Figure 3(b) shows the center-of-mass angular distribution for the Δ^+ with appropriate background subtraction. As with the Δ^{++}, it is definitely backward-peaked. The distribution in four-momentum transfer to the Δ^+ [Fig. 3(c)] indicates an excess of events over background below 1300 MeV/c. The decay angular distribution for the Δ^+ has been studied for various cuts on four-momentum transfer with the exclusion of other resonances involving the same particles. In all cases, the decay angular distributions are quite consistent with isotropy. Figure 3(d) is the Δ^+ decay distribution for low-four-momentum-transfer events (K^{*-} removed).

B. $K\pi$ Resonances

1. $\bar{K}^{*0}$

In Fig. 4(a) is shown the $K^-\pi^+$ effective-mass distribution. The $\bar{K}^{*0}(890)$ signal is a 10-standard-deviation enhancement over background. We see no evidence for $K_V(1420)$ here. The center-of-mass angular distribution for the $\bar{K}^{*0}(890)$ is shown in Fig. 4(d). It is peaked forward, though the effect is not so significant as the backward peaking of the Δ^{++} and Δ^+. Also, the four-momentum-transfer distribution for the $\bar{K}^{*0}$ [Fig. 4(c)] departs less from background than do the corresponding distributions for the Δ^{++} and Δ^+. The $\bar{K}^{*0}$ decay angular distribution is shown in Fig.

4(b). It is quite flat, having a χ^2 probability of 0.7 for an isotropic fit.

2. K^{*-}

Figure 5(a) shows the $K^-\pi^0$ mass distribution. A 5.5-standard-deviation enhancement near 900 MeV is assumed to be the $K^{*-}(890)$. No other significant effects are observed in this channel. The center-of-mass angular distribution for the $K^{*-}(890)$ [Fig. 5(b)] is forward-peaked, though less than for the $\bar{K}^{*0}(890)$. The $K^{*-}(890)$ decay angular distribution is presented in Fig. 5(d). There is some indication of a preference for a sine-square dependence.

C. Dipion Spectra

1. $\pi^-\pi^0$

The $\pi^-\pi^0$ mass distribution is displayed in Fig. 9(b). The ρ^- is a 3-standard-deviation enhancement. The experimental peak width given in Table II for the ρ^- (100 MeV) is smaller than the currently accepted intrinsic width. The distribution has been fitted both with the width included as an adjustable parameter and also with it fixed at its accepted value. The ρ^- contribution is 3.5% in the former instance and 5.5% in the latter. The fitted curve in either case is slightly undernormalized in the peak of phase space and overnormalized in the tail. Thus, the amount of ρ^- determined by the fit is probably an underestimate. The 3.5% ρ^- contribution is considered a lower limit. A search has been made for contributions from resonances

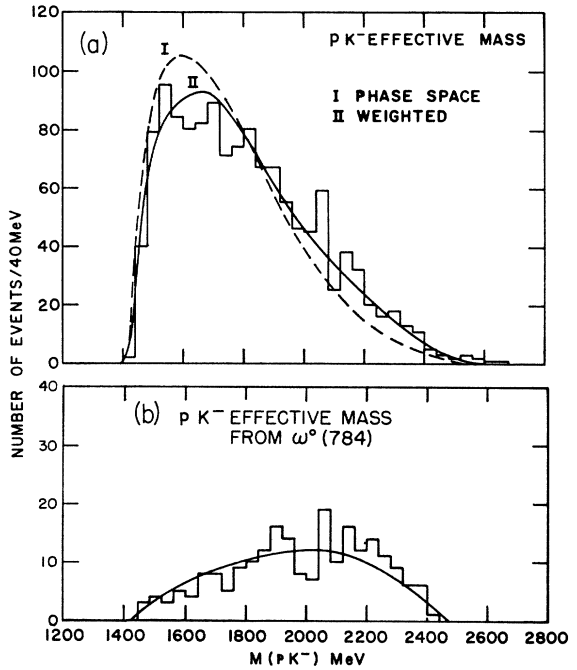

FIG. 7. Gross K^-p effective-mass distribution (a) for reaction (1) and K^-p mass spectrum for ω^0 events (b).

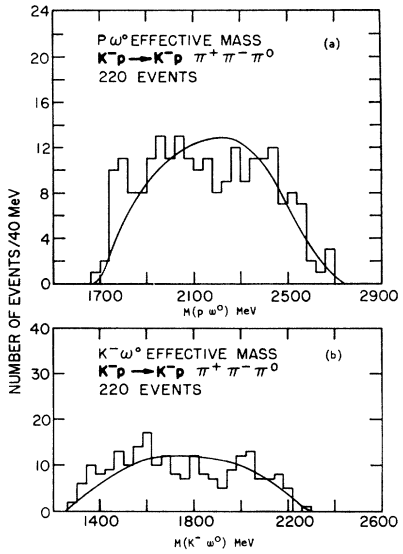

FIG. 8. Effective-mass distributions from reaction (1) for $p\omega^0$ and $K^-\omega^0$.

decaying into ρ^- and one or more other particles. It is observed that events in the A_1^0 region (1060±60 MeV) of the $\pi^+\pi^-\pi^0$ distribution are strongly associated with the ρ^-.

2. $\pi^+\pi^0$

The only important feature of the $\pi^+\pi^0$ mass distribution [Fig. 9(c)] is the $\rho^+(760)$, a 5-standard-deviation effect. As indicated below, approximately 60% of the ρ^+ is contributed through decay of the A_1^0. Results of investigation of the $p\rho^+$ and $K^-\rho^+$ distributions are presented in Table III. We conclude that the ρ^+ arises essentially as the decay product of other resonances, principally the A_1^0, an 1820 $p\rho^+$ effect, and the $K_N(1420)$. The estimated number of events in these three effects is consistent with the ρ^+ contribution in the gross distribution.

D. 3π Effects

The $\pi^+\pi^-\pi^0$ mass distribution is presented in Fig. 6(a). We have good evidence for the $\eta(548)$, a 4-standard-deviation effect in our data, and for the $\omega^0(784)$, which is a 13-standard-deviation enhancement. A fit to the distribution including Breit-Wigner terms for these two resonances plus weighted phase space yields a χ^2 probability of 0.2. There remains an excess of events over background in the 1060-MeV region, which we interpret as due to production of the A_1^0.[10]

[10] The possible contribution of the $\varphi(1019)$ meson in our data has been considered. The broad effect centered at ~1060 MeV in both the gross 3π and $\rho^\pm\pi^\mp$ distribution argues against a significant presence of the narrow ($\Gamma \cong 3$ MeV) φ. Furthermore, no clear ρ^0 signal for events in the A_1^0 band is noted. Also, the number of fits to $K^-pK^+K^-$ in our data is less than 20, which, used with φ branching ratios from Rosenfeld's tables, implies less than seven events involving $\varphi \to \rho^\pm\pi^\mp$.

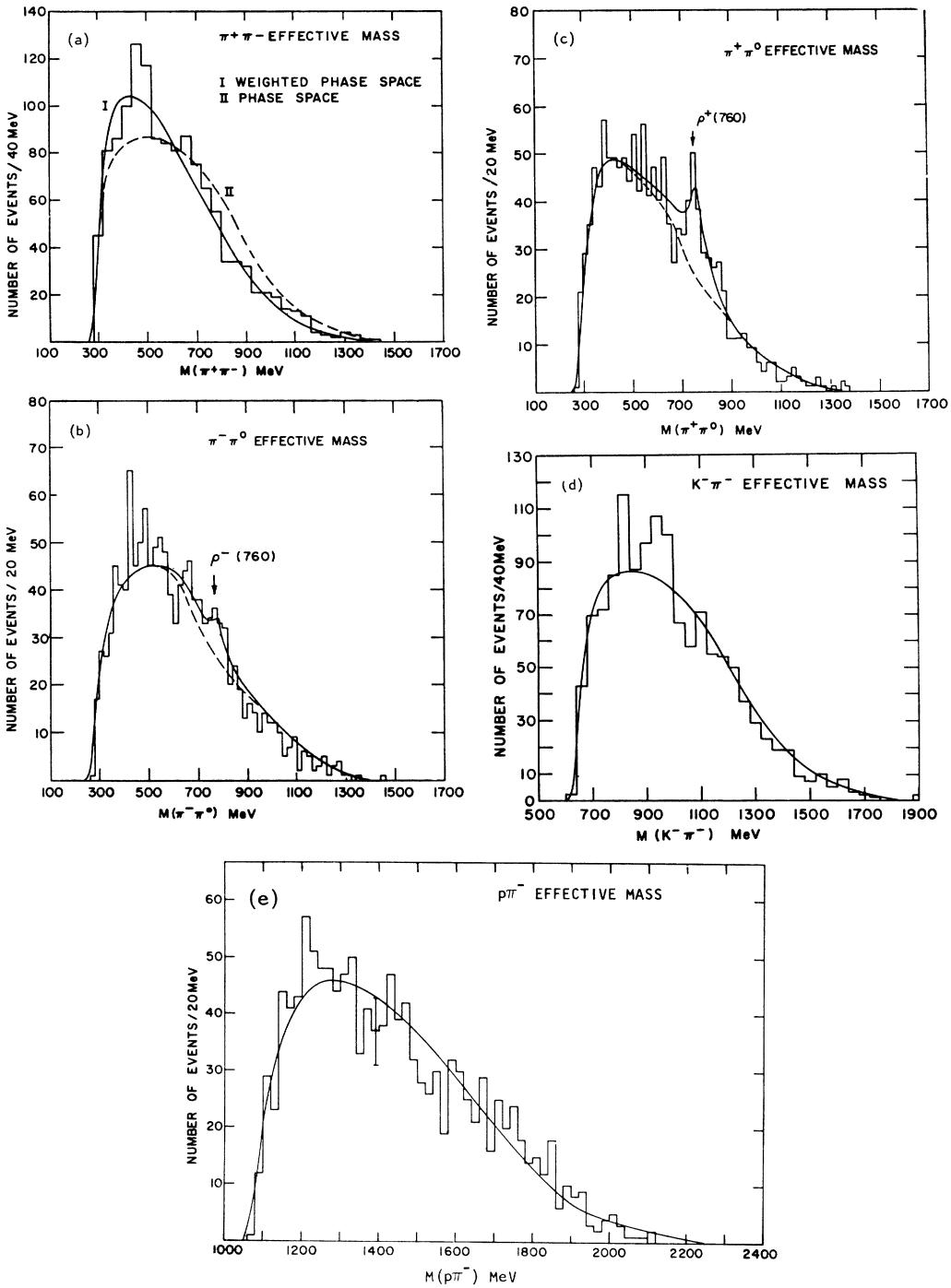

FIG. 9. Two-body mass distributions for reaction (1). For $p\pi^+$, $p\pi^0$, $K^-\pi^+$, $K^-\pi^0$, and K^-p mass distributions see Figs. 2(a), 3(a), 4(a), 5(a), and 7(a), respectively.

There is evidence in the gross $\pi^+\pi^-\pi^0$ distribution for two other effects, one at 960 MeV and the other at 1320 MeV, which is in the region of the $A_2(1300)$. The 960-MeV effect and the A_2^0 are 2.5- and 1.5-standard-deviation effects, respectively. We have fitted the gross $\pi^+\pi^-\pi^0$ mass distribution using, in turn, three, four, or five resonance terms. The χ^2 probabilities range from 0.85 to 0.90 for the three fits. The χ^2 probability for the three-resonance fit including the η, ω^0, and A_1^0 is 0.85. There is very little sensitivity for the 960-MeV

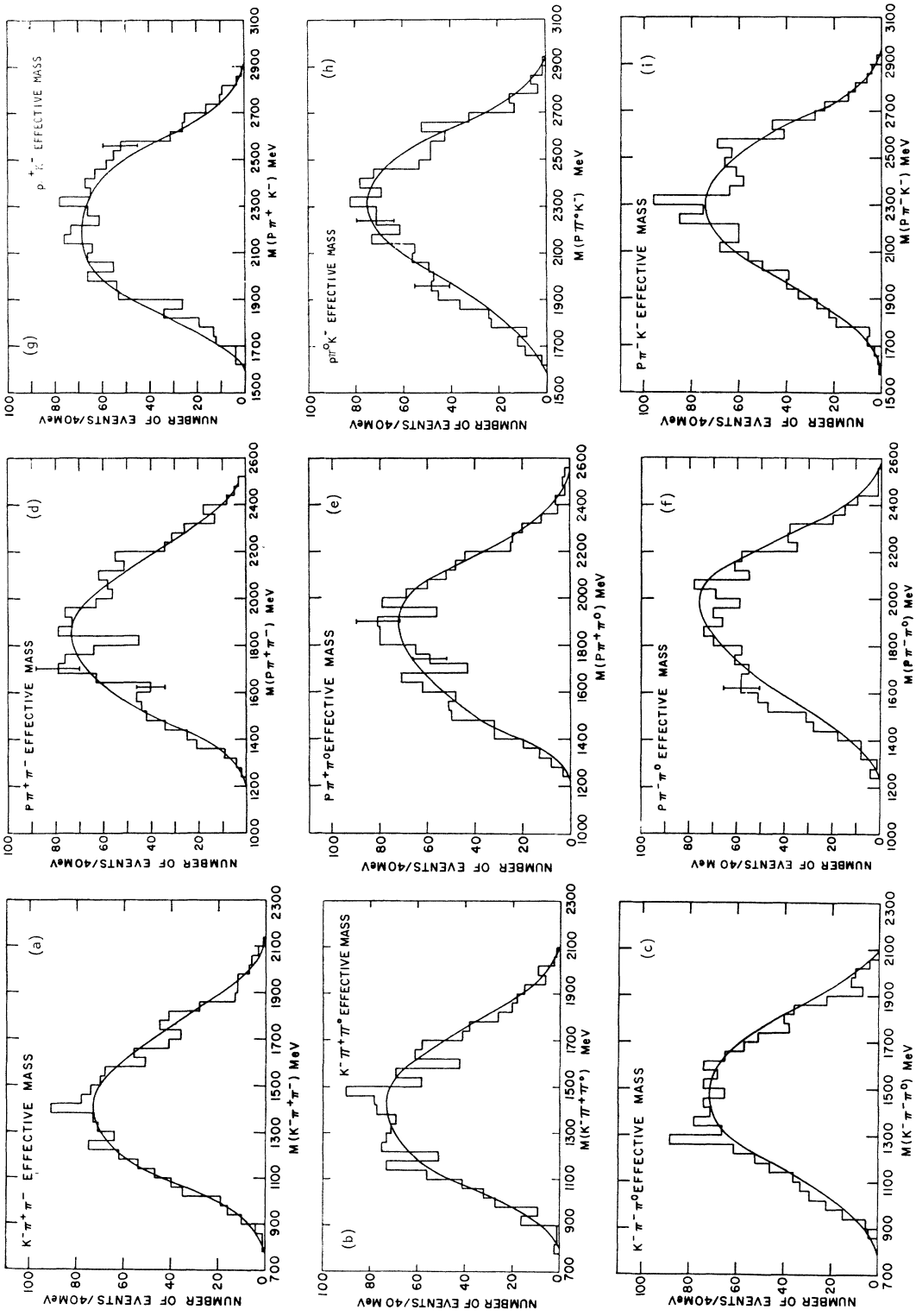

FIG. 10. Three-body mass distributions for reaction (1). For $\pi^+\pi^-\pi^0$ mass distribution see Fig. 6(a).

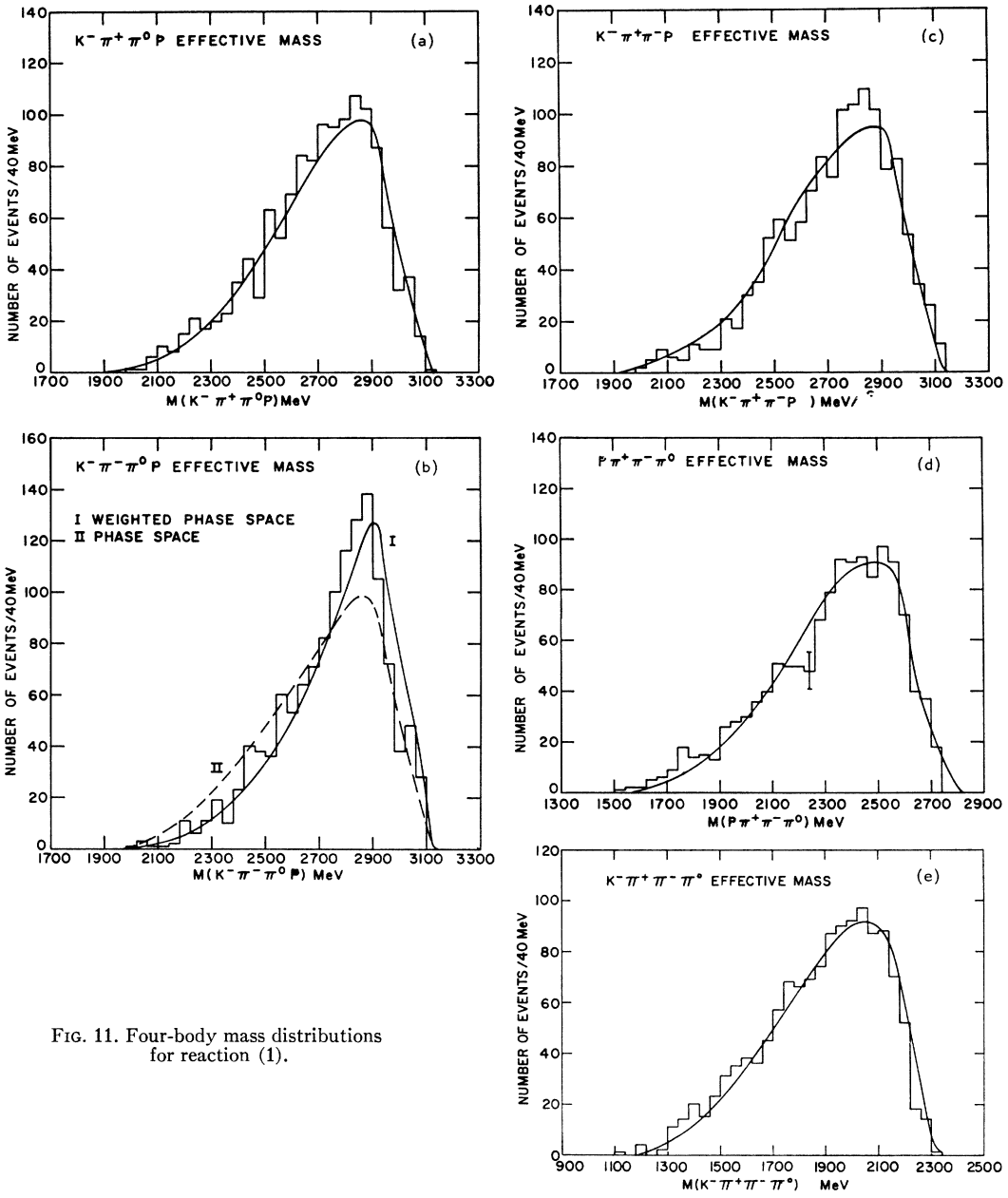

FIG. 11. Four-body mass distributions for reaction (1).

feature and/or the A_2. The fit shown in Fig. 6(a) is the five-resonance fit, including Breit-Wigner terms for the η, ω, the 960-MeV effect, the A_1^0, and A_2^0. A discussion of the 960-MeV feature seen here [in conjunction with a similar effect in the $\pi^+\pi^+\pi^-$ distribution of reaction (2)] is presented elsewhere.[11]

1. A_1^0

Discussions of certain aspects of the A_1^0 effect in our data have been presented in previous papers.[12,13] We do not review all of those arguments here. However, there are some features not covered previously which we wish to discuss here. For completeness we include in Figs. 6(b)–6(d), respectively, the $\rho^{\pm}\pi^{\mp}$ distribution from reaction (1), the $\pi^{\pm}\pi^0$ mass projection from the folded $\pi^+\pi^0$-$\pi^-\pi^0$ mass-scatter plot for A_1^0 events, and

[11] R. E. Juhala, R. A. Leacock, J. I. Rhode, J. B. Kopelman, L. M. Libby, and E. Urvater, Phys. Letters **27B**, 257 (1968).

[12] R. E. Juhala, R. A. Leacock, J. I. Rhode, J. B. Kopelman, L. M. Libby, and E. Urvater, Phys. Rev. Letters **19**, 1355 (1967).

[13] R. E. Juhala, R. A. Leacock, J. I. Rhode, J. B. Kopelman, L. M. Libby, and E. Urvater, in Proceedings of the Third Topical Conference on Resonant Particles, Athens, Ohio, 1967 (unpublished).

the $\pi^+\pi^-$ mass distribution for A_1^0 events.[14] The mass of the A_1^0 determined from fits to the gross $\pi^+\pi^-\pi^0$ distribution and presented in Table II is about 12 MeV higher than that obtained in Ref. 12 from the same distribution. This arises from the addition of a resonance term in the fit for a possible effect at 960 MeV. The width and relative contribution of the A_1^0 are not significantly affected. The best estimate of the A_1^0 mass, 1064 MeV, was obtained[12] from fits to the $\rho^\pm\pi^\mp$ distribution. This value is closer to the 1069-MeV mass quoted in Table II. In our previous analysis the effect on the $\pi^+\pi^-\pi^0$ spectrum of removal of other strong resonances, e.g., $\bar{K}^{*0}$, Δ^{++}, Δ^+, and K^{*-}, was not considered. We note here that the shape of the 3π distribution is little changed by removal of Δ^+ or K^{*-}, but that excluding either or both $\bar{K}^{*0}$ and Δ^{++} leads to a relative enhancement of the A_1^0 effect. We conclude that the A_1^0 in our data is not produced significantly in conjunction with these other states.

We have studied the production characteristics of the A_1^0 in several ways. The center-of-mass (c.m.) angular distribution of the A_1^0 is presented in Fig. 12(g). This is the same distribution as shown in Ref. 12. By A_1^0 events we mean events with $\pi^+\pi^-\pi^0$ mass in the A_1^0 region (1060±60 MeV) and $\pi^+\pi^0$ and/or $\pi^-\pi^0$ mass in the ρ region (760±60 MeV). A distinct forward preference is indicated in this distribution. A "background" distribution formed for events in the A_1^0 region but with $\pi^\pm\pi^0$ mass *outside* the ρ bands is presented in Fig. 12(h). This distribution also has an excess of events in the forward direction, but the effect is weaker and of a qualitatively different character than that for A_1^0 events. Figure 12(i) gives an approximate reconstruction of the true c.m. angular distribution for A_1^0 events based on estimates of relative signal-to-background ratios in both the "A_1^0" and "background" cuts. This is a more sophisticated form of background correction than that applied in other cases in this paper; however, the results here are not strongly dependent on the use of this procedure. Our conclusion is that the A_1^0 is produced preferentially in the forward direction in the c.m. system.

The c.m. angular distribution of the recoiling proton for A_1^0 events [Fig. 12(a)] is considerably more striking. We note a sharp accumulation of events for $\cos\theta \leq -0.8$. The association of this feature with the A_1^0 is evident from Fig. 12(b), which shows two different background estimates, one (curve I) for events in the A_1^0 region, but with $\pi^\pm\pi^0$ mass *outside* the ρ bands, and the other (curve II) for events above and below the A_1^0 band, but with $\pi^\pm\pi^0$ mass *inside* the ρ bands. Neither distribution exhibits the strong backward peaking of Fig. 12(a), and, indeed, the small remaining spike for $\cos\theta \leq -0.8$ in each may be considered to be contributed largely from A_1^0 events outside the specific A_1 cuts. A reconstruction of the "true" proton c.m. angular distribution for A_1^0 events [Fig. 12(c)] according to the same method dscussed above further emphasizes the backward peak. This same effect is reflected again in the distribution in four-momentum transfer $(-t)$ from target to final-state proton for A_1^0 events [Fig. 12(j)], which exhibits a large spike at low $|t|$ values. We conclude that the mechanism responsible for production of the A_1^0 in this reaction is characterized by low-momentum transfer to the proton, much lower than that for other processes contributing to the background.

The c.m. angular distribution of the K^- for A_1^0 events [Fig. 12(d)] is forward-peaked, as is the background. Here again, however, the distribution for A_1^0 events is rather more sharply forward-peaked than that for background events, though the effect is not so striking as that for the proton.

In Ref. 12, two different approaches were applied in an attempt to determine the A_1 spin and parity. Both methods are based on work of Berman and Jacob.[15,16] In one procedure a particular moment R of the experimental joint angular distribution for the sequential decay $A_1^0 \to \rho\pi$, $\rho \to \pi\pi$ is calculated. Specifically, we have

$$R = \int I(\theta,\varphi,\theta',\varphi')(5\cos^2\theta' - 1)d\Omega d\Omega'.$$

Here θ and φ are the polar and azimuthal angles, respectively, of the ρ momentum vector in the A_1^0 rest frame, referred to a coordinate system in which the z axis is the incident K^- momentum (again in the A_1^0 rest frame) and the y axis is the normal to the A_1^0 production plane. The angles θ' and φ' are the polar and azimuthal angles of one of the two pions from the ρ decay in the ρ rest frame, referred to a coordinate system in which the z axis is the ρ momentum vector and the y axis is the normal to the ρ production plane. These coordinate systems are indicated in Fig. 13. As indicated in Ref. 15, the 00 element ρ_{00} of the spin-density matrix of the ρ meson (considered as a function of θ and φ) is given as

$$\rho_{00}(\theta,\varphi) \sim \int I(\theta,\varphi,\theta',\varphi')(5\cos^2\theta' - 1)d\Omega'.$$

Thus we have

$$R \sim \int \rho_{00}(\theta,\varphi)d\Omega.$$

When $\rho_{00}(\theta,\varphi)$ is evaluated using the theoretical expression for $I(\theta,\varphi,\theta',\varphi')$, it is found that $\rho_{00}(\theta,\varphi)=0$ for $J^P=0^+$, 1^-, 2^+, which implies $R=0$. Inverting this argument, we obtain the result that a nonzero experi-

[14] The distributions pertaining to the A_1^0 investigations [Figs. 6(b)–6(d) and 12(a)–12(l)] are from an earlier 1700-event sample for which the azimuthal-angle–vertex-position cut (see Ref. 5) was not used. A reexamination of certain of these distributions with this cut included indicates that the results are not sensitive to this variation in data treatment.

[15] S. M. Berman and M. Jacob, Stanford Linear Accelerator Report No. 43, 1965 (unpublished).

[16] S. M. Berman and M. Jacob, Phys. Rev. **139**, B1023 (1965).

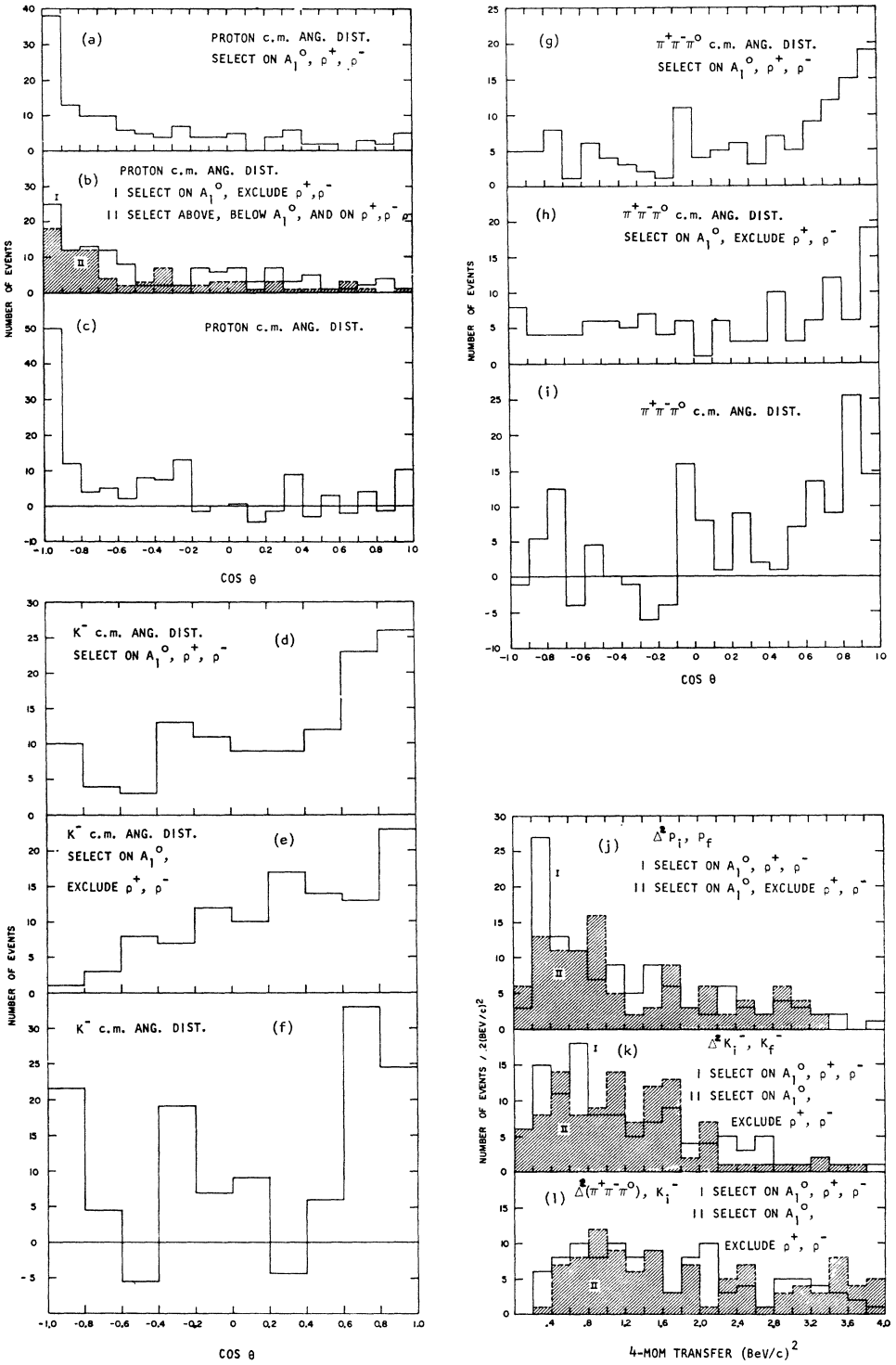

FIG. 12. A_1^0 and related c.m. angular distributions and four-momentum-transfer distributions. Histogram (c) is a linear combination of histograms (a) and (b)I—specifically, 2.31 (a)−1.54 (b)I. Similarly, (f) is formed from (d) and (e), and likewise (i) from (g) and (h).

mental value of R, i.e., an R value differing significantly from zero in relation to the assigned error, implies the spin-parity sequence 0^-, 1^+, 2^-, ...

A sample of 119 events having $\pi^+\pi^-\pi^0$ mass in the A_1^0 region (1060±60 MeV) and $\pi^+\pi^0$ or $\pi^-\pi^0$ mass in the ρ region (760±60 MeV) was used in this analysis.

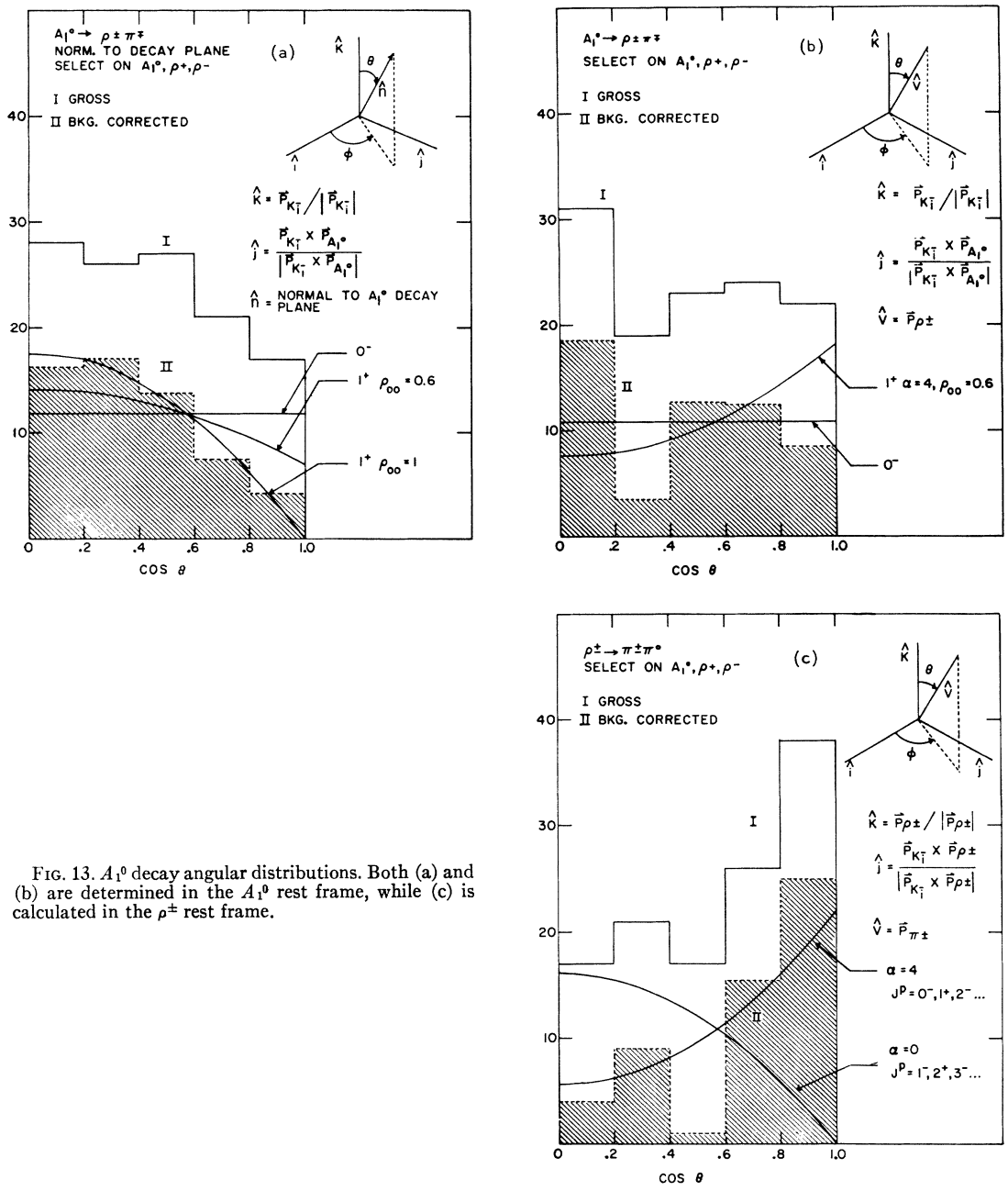

FIG. 13. A_1^0 decay angular distributions. Both (a) and (b) are determined in the A_1^0 rest frame, while (c) is calculated in the $\rho^\pm$ rest frame.

Events in the ρ^+, ρ^- overlap region were excluded. Background effects were estimated on the assumption that the characteristics of background within the ρ bands are adequately represented by distributions for events outside the ρ bands. The signal-to-background ratio within the ρ bands is approximately 1:1, on the basis of fits to the $\rho^\pm\pi^\mp$ mass spectrum. An experimental R value of 1.7 ± 0.5 was obtained, which, from the preceding arguments, implies that the A_1 spin-parity is restricted to 0^-, 1^+, 2^-, ... This result is not sensitive to variations in background treatment. Those features of the data which are characterized by the nonzero value of R can also be displayed via the distribution in $\cos\theta'$, the polar angle in the $\rho \to \pi\pi$ decay. The theoretical expression for this distribution is $I(\theta') \sim \rho_{00} \cos^2\theta' + \rho_{11} \sin^2\theta'$, where ρ_{00} is proportional to R. The experimental distribution [Fig. 13(c)] exhibits a strong $\cos^2\theta'$ dependence (i.e., contains a large $\cos^2\theta'$ contribution) both before and after background subtraction, while $R=0$ implies a pure $\sin^2\theta$ form. The χ^2 probability for a $\sin^2\theta$ fit to this distribution is $\sim 4\%$. The restriction of the spin-parity of

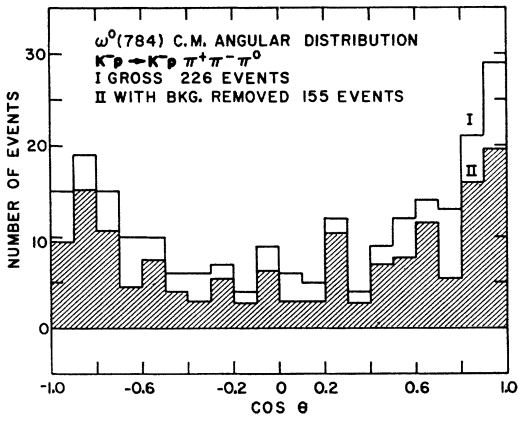

FIG. 14. Center-of-mass angular distribution for ω^0.

the A_1 to 0^-, 1^+, 2^-, ..., is based entirely on the $\cos\theta'$ distribution for $\rho \rightarrow \pi\pi$.

The second method involves an examination of the polar angular distribution of the normal to the A_1^0 decay plane. This is calculated in the A_1^0 rest frame, referred to the incident K^- direction seen in that system. The same cuts on 3π and $\pi\pi$ masses used in the preceding analysis are applied here to define A_1 and background events. The experimental data are presented in Fig. 13(a). The distribution without background correction indicates a sine-squared dependence which is further enhanced after subtraction of background. For an A_1^0 spin-parity of 0^-, a flat distribution $[I(\beta)=\text{const}]$ is predicted, while for 1^+ the form $I(\beta)\sim(1+\rho_{00})+(1-3\rho_{00})\cos^2\beta$ is given, where ρ_{00} is the appropriate A_1^0 spin-density matrix element. The experimental distribution with background correction is fitted best with the 1^+ form for $\rho_{00}=1$. The χ^2 probabilities for the 0^- and 1^+ fits are 43 and 98%, respectively. Assuming that 1^+ is the correct assignment, we infer from this only that a large value for ρ_{00} (≥ 0.5) is implied.

From these two analyses we conclude that our results strongly favor an A_1^0 spin-parity in the sequence 0^-, 1^+, 2^-, ..., and that they are consistent with the previously favored 1^+ assignment.

2. ω^0 and Related Effects

In an investigation of the $K^-\pi^-\pi^+\pi^0 p$ final state in K^-p interactions at 3.8 BeV/c, Carmony *et al.*[1] found

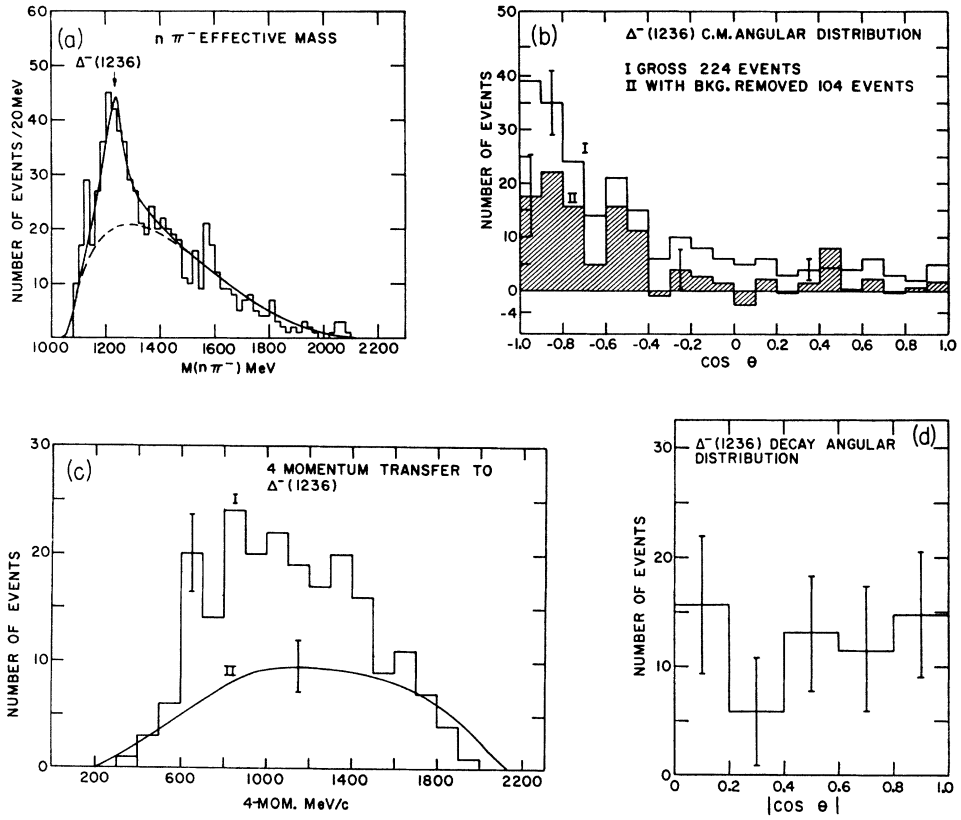

FIG. 15. Effective-mass distribution for $n\pi^-$ system from reaction (2), and angular and four-momentum-transfer distributions for Δ^-. In (c), I is the histogram for Δ^- events and II is the background shape determined from corresponding distributions for events with $n\pi^-$ mass adjacent to the Δ^- band. The Δ^- decay angular distribution (d) is for a subsample of Δ^- events for which the four-momentum transfer from the target proton to outgoing $n\pi^-$ system is less than 1100 MeV/c. A background correction has been applied. Angles in (d) are referred to the target-proton direction seen in the Δ^- rest frame.

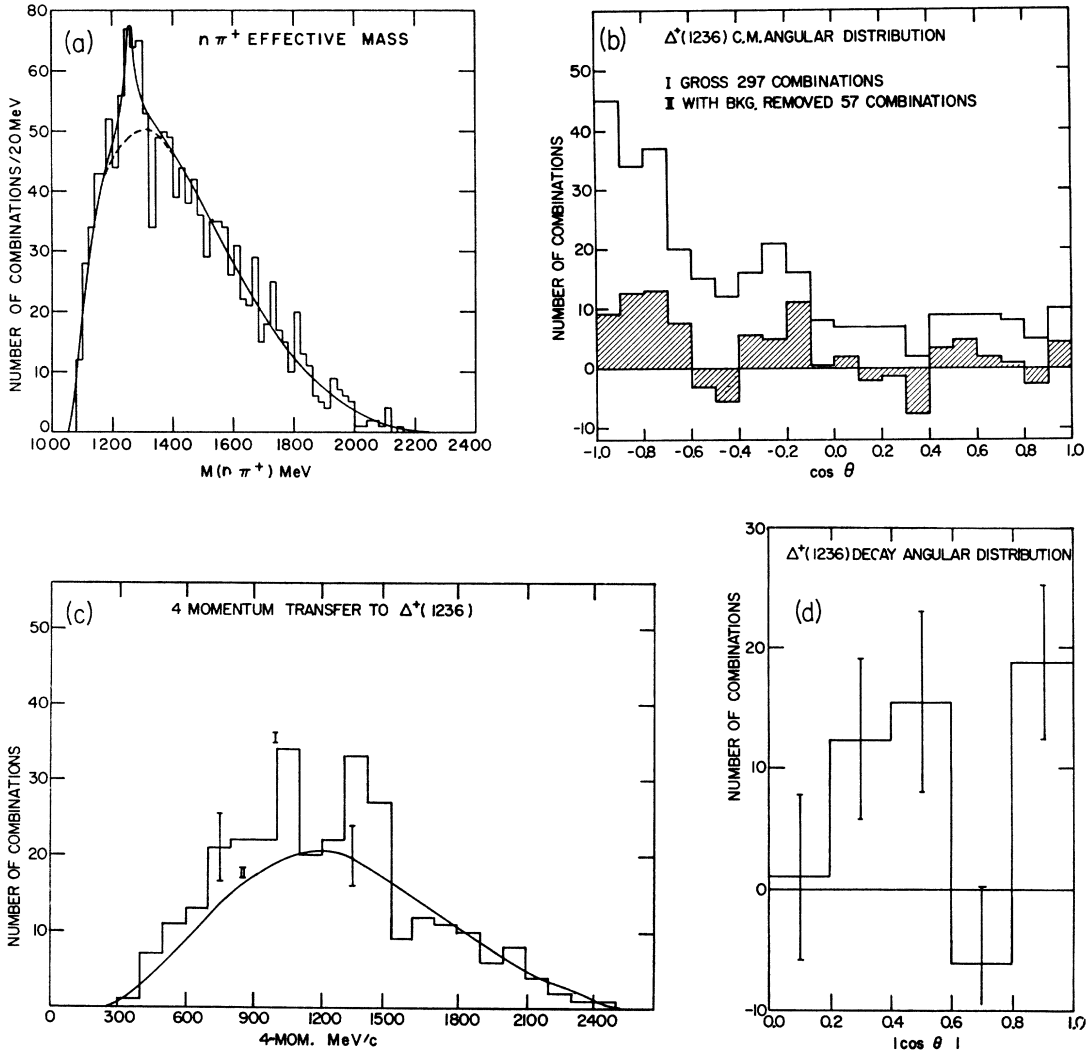

FIG. 16. Effective-mass distribution of $n\pi^+$ system for reaction (2) and angular and momentum-transfer distributions for Δ^+. In (c), I is the histogram for Δ^+ events and II is the background shape determined from corresponding distributions for events with $n\pi^+$ mass adjacent to the Δ^+ band. The Δ^+ decay angular distribution (d) is for a subsample of Δ^+ events from which $\bar{K}^{*0}$ events have been removed and for which the four-momentum transfer between the target proton and outgoing $n\pi^+$ system is less than 1100 MeV/c. A background correction has been applied. Angles for (d) are referred to the target-proton direction seen in the Δ^+ rest frame.

good evidence for $\omega^0 Y_0^*(1520)$, $\omega^0 Y_0^*(1815)$, and $\omega^0 Y_0^*(2100)$ production. In their data the cross section for all ω^0 production was 76 ± 11 μb, of which 70 μb were contributed by the $\omega^0 Y^*$ channels. At our higher beam momentum, however, we see essentially no evidence for this kind of process, though the ω^0 cross section has increased to 120 ± 25 μb. Figures 7(a) and 7(b) show the gross K^-p mass spectra and the selected distribution for ω^0 events, respectively. Appropriate weighted-phase-space comparison curves are shown.

We have also examined the $K^-\omega^0$ and $p\omega^0$ mass distributions (Fig. 8). The former exhibits weak enhancements near the ends of the distribution, with a depopulation in the central region. In the 3.8-BeV/c work of Carmony *et al.*,[1] evidence was seen for possible effects at $\approx$1400 and 1660 MeV. The statistical reliability of the data in the current paper does not permit a confirmation of this. The $p\omega^0$ mass distribution has something of the same character as the $K\omega^0$, i.e., a deficiency of events in the central region with enhancements at the ends. In particular, we note a 2.5-standard-deviation effect at 1780 MeV (just above threshold). Evidence for a $p\omega^0$ effect near this mass has been reported elsewhere.[17]

The ω^0 c.m. angular distribution is shown in Fig. 14. A symmetric forward and backward peaking is evident.

[17] P. L. Connolly, W. E. Ellis, P. V. C. Hough, D. J. Miller, F. W. Morris, C. Ouannes, R. S. Panvini, and A. M. Thorndike, in Proceedings of the Third Topical Conference on Resonant Particles, Athens, Ohio, 1967 (unpublished).

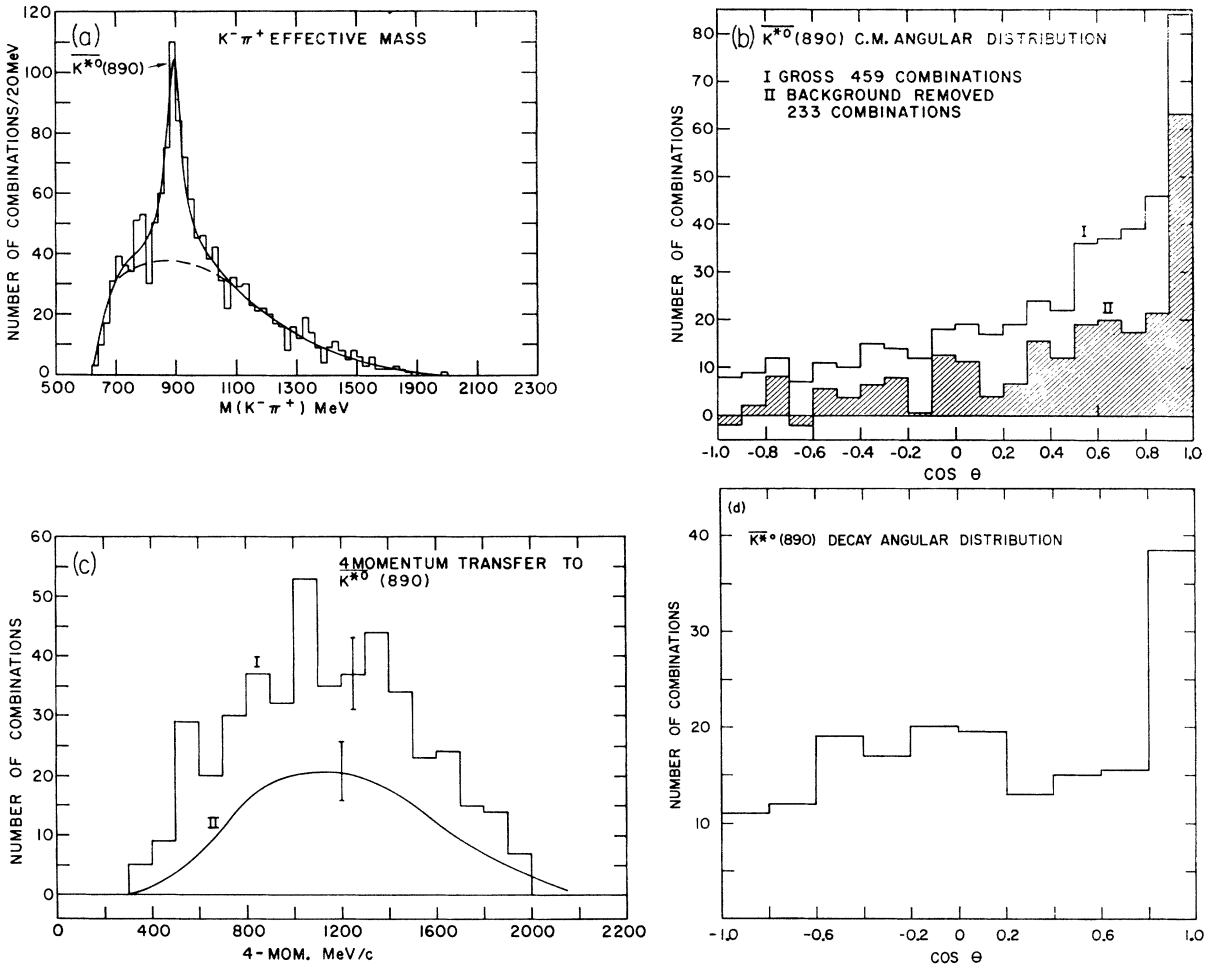

FIG. 17. Effective-mass distribution of $K^-\pi^+$ system for reaction (2) and angular and momentum-transfer distributions for $\bar{K}^{*0}$. In (c), I is the histogram for $\bar{K}^{*0}$ events and II is the background shape determined from corresponding distributions for events with $K^-\pi^+$ mass adjacent to the $\bar{K}^{*0}$ band. The $\bar{K}^{*0}$ decay angular distribution (d) is for a subsample of $\bar{K}^{*0}$ events for which the four-momentum transfer between the projectile and outgoing $K^-\pi^+$ system is less than 1200 MeV/c. A background correction has been applied. There is no correction in (d) for events with both combinations in the $\bar{K}^{*0}$ band. Angles in (d) are referred to the projectile direction seen in the $\bar{K}^{*0}$ rest frame.

The angular distribution (not shown) of the normal to the ω^0 decay plane (referred to the incident K^- direction seen in the ω^0 rest frame) has been examined for the complete sample of ω^0 events and separately for forward-going and backward-going ω^0's. There is no striking difference between these distributions; they are all consistent with isotropy.

IV. $K^-\pi^-\pi^+\pi^+n$ FINAL STATE

Results of fitting procedures for the 18 channels available in this final state are presented in Table II. Procedures are generally analogous to those previously described save in the case of channels involving a single π^+, for which there are two combinations per event. In determining resonance contributions in such channels, additional corrections for possible double counting of resonance events have been applied. The gross effective-mass distributions for this final state are presented in Figs. 15–20.

A. Baryon Resonances

Figure 15(a) shows the $n\pi^-$ effective-mass distribution. The $\Delta^-(1236)$ enhancement is a 7-standard-deviation effect. Distributions in four-momentum transfer ($\sqrt{-t}$) and c.m. angle for the Δ^- are shown in Figs. 15(c) and 15(b), respectively. We have investigated the decay angular correlations for this resonance for various four-momentum-transfer cuts, with the exclusion of Δ^+ or $\bar{K}^{*0}$ events. A symmetric decay distribution is obtained only when $\bar{K}^{*0}$ events are excluded. In this case the χ^2 probability for an isotropic fit is 0.91.

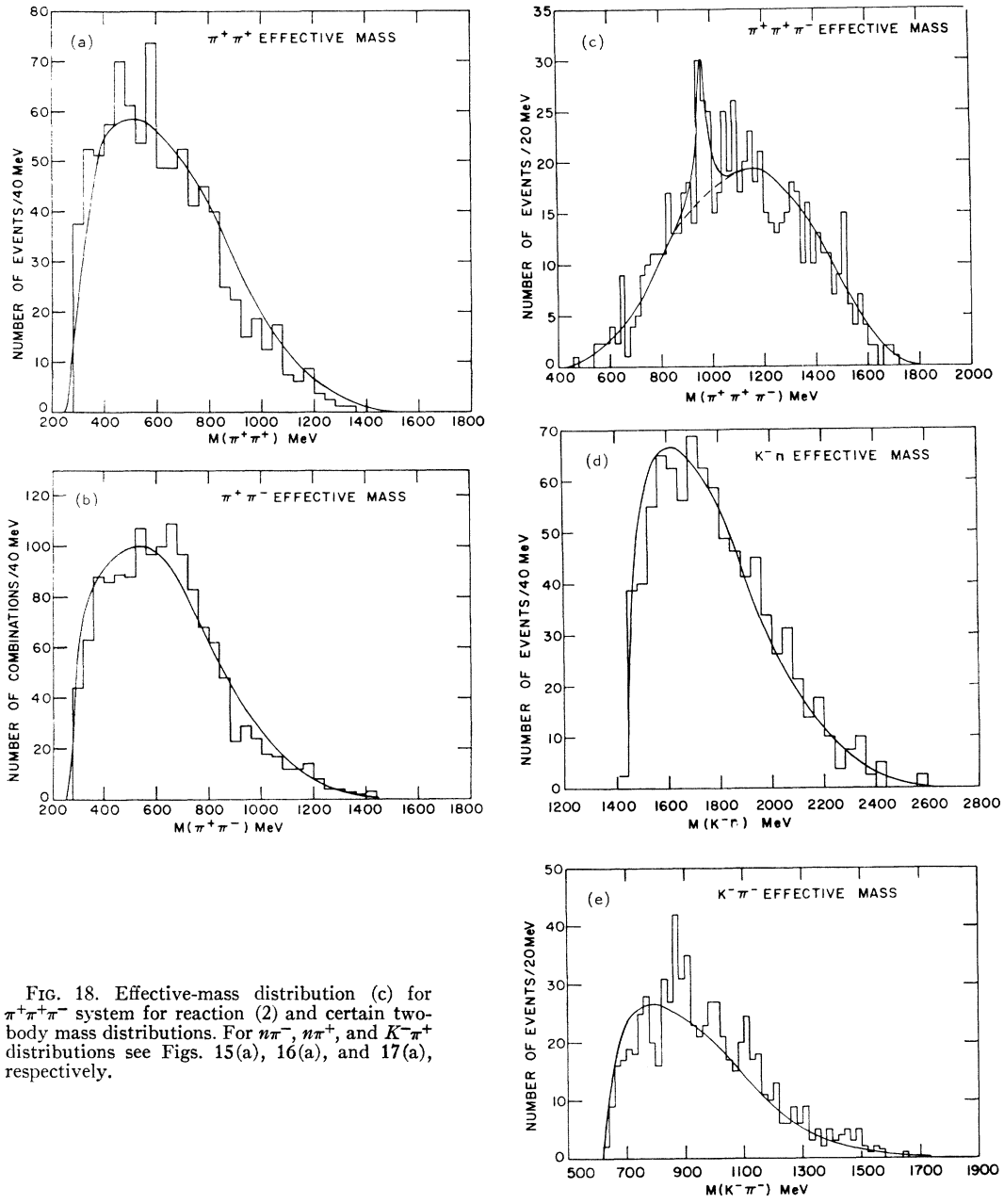

FIG. 18. Effective-mass distribution (c) for $\pi^+\pi^+\pi^-$ system for reaction (2) and certain two-body mass distributions. For $n\pi^-$, $n\pi^+$, and $K^-\pi^+$ distributions see Figs. 15(a), 16(a), and 17(a), respectively.

The $n\pi^+$ distribution is shown in Fig. 16(a). A 3.4-standard-deviation enhancement over weighted phase space centered at 1260 MeV is interpreted as the $\Delta^+(1236)$, though the mass is noticeably greater than the expected value. The persistence of an effect in this region after exclusion of $\bar{K}^{*0}$ or Δ^- events is a further confirmation that this is not merely a reflection of these two strong resonances. The c.m. angular distribution for the Δ^+ is shown in Fig. 16(b). It exhibits a definite backward peaking. The distribution in four-momentum transfer $(\sqrt{-t})$ to the Δ^+ [Fig. 16(c)] indicates a slight excess of events over background below 1500 MeV/c. The decay angular distribution [Fig. 16(d)] has been investigated with various cuts on four-momentum transfer and excluding other resonances. The distributions are symmetric about 90° only with exclusion of $\bar{K}^{*0}$ events. The χ^2 probability in this case is 0.75 for an isotropic fit and 0.65 for a fit including a $\cos^2\theta$ component.

B. $K\pi$ Effects

The strongest effect in the $K^-\pi^-\pi^+\pi^+ n$ final state is the $\bar{K}^{*0}$, which forms an 11-standard-deviation enhancement in the $K^-\pi^+$ distribution [Fig. 17(a)].

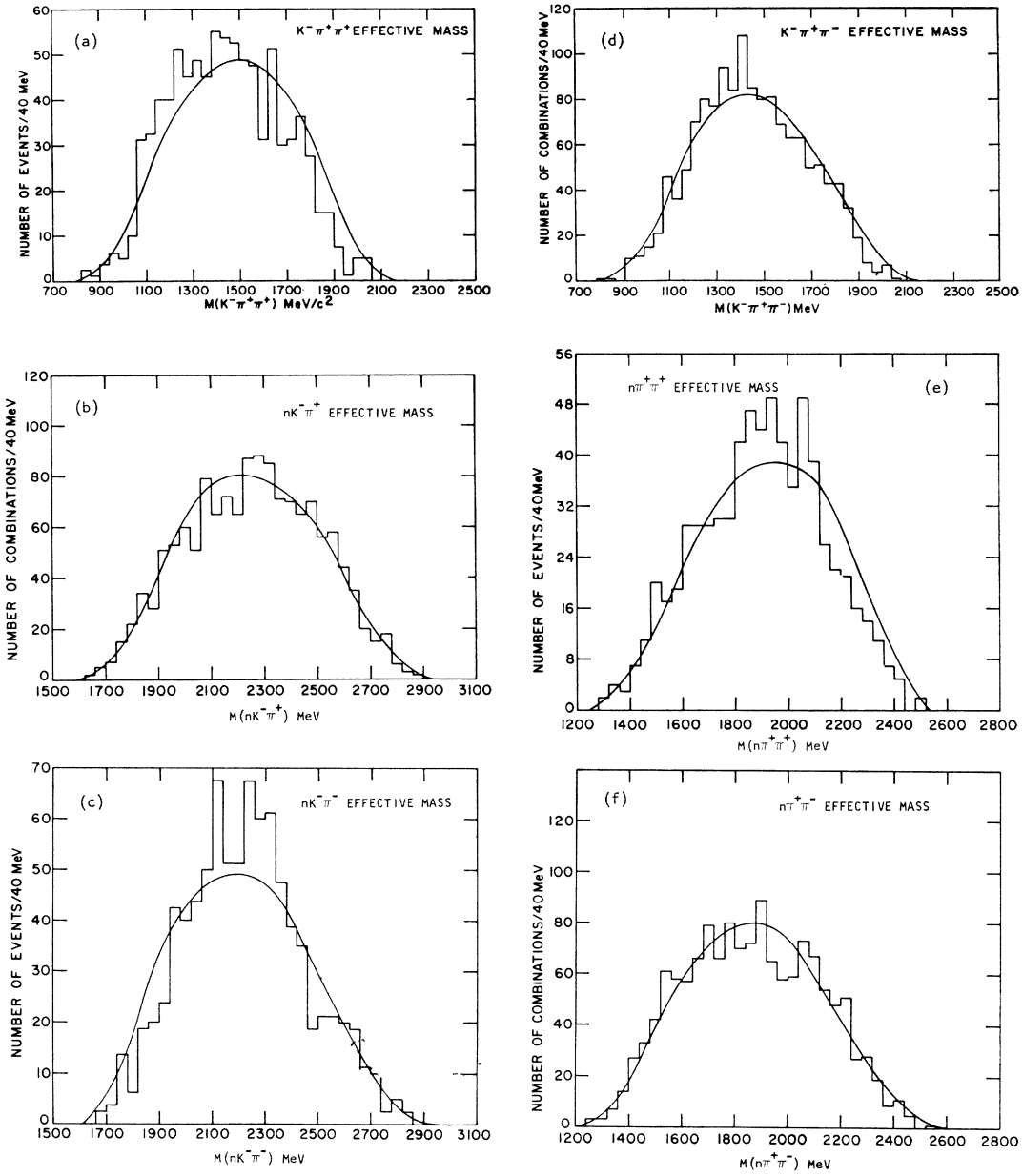

FIG. 19. Three-body mass distributions for reaction (2). For $\pi^+\pi^+\pi^-$ distribution see Fig. 18(c).

The c.m. angular distributions and four-momentum-transfer distributions for the $\bar{K}^{*0}$ are shown in Figs. 17(b) and 17(c), respectively. Neither distribution differs remarkably from that for the background.

The decay angular distribution of the $\bar{K}^{*0}$ has been studied for events having four-momentum transfer both less than and greater than 1200 MeV/c, with and without exclusion of $\Delta^+(1236)$ events. The decay angular distributions for events with four-momentum transfer greater than 1200 MeV/c are symmetric, with χ^2 probabilities for isotropic fits of 0.60 and 0.45. For four-momentum transfer less than 1200 MeV/c the distributions show a forward peak for the cosine of the decay angle greater than 0.8. Removal of Δ^+ events has no significant effect on the distributions. Events with both $K^-\pi^+$ mass combinations in the region 900 ± 60 MeV are also forward-peaked in the decay angle, whereas events with both combinations in the respective background cuts show no forward peaking. Removal of events with double combinations leads to a substantial reduction of this forward peak. With the exception of this peak, however, these decay distributions indicate a $\sin^2\theta$ contribution. Figure 17(d) shows the $\bar{K}^{*0}$ decay angular distribution for low-four-

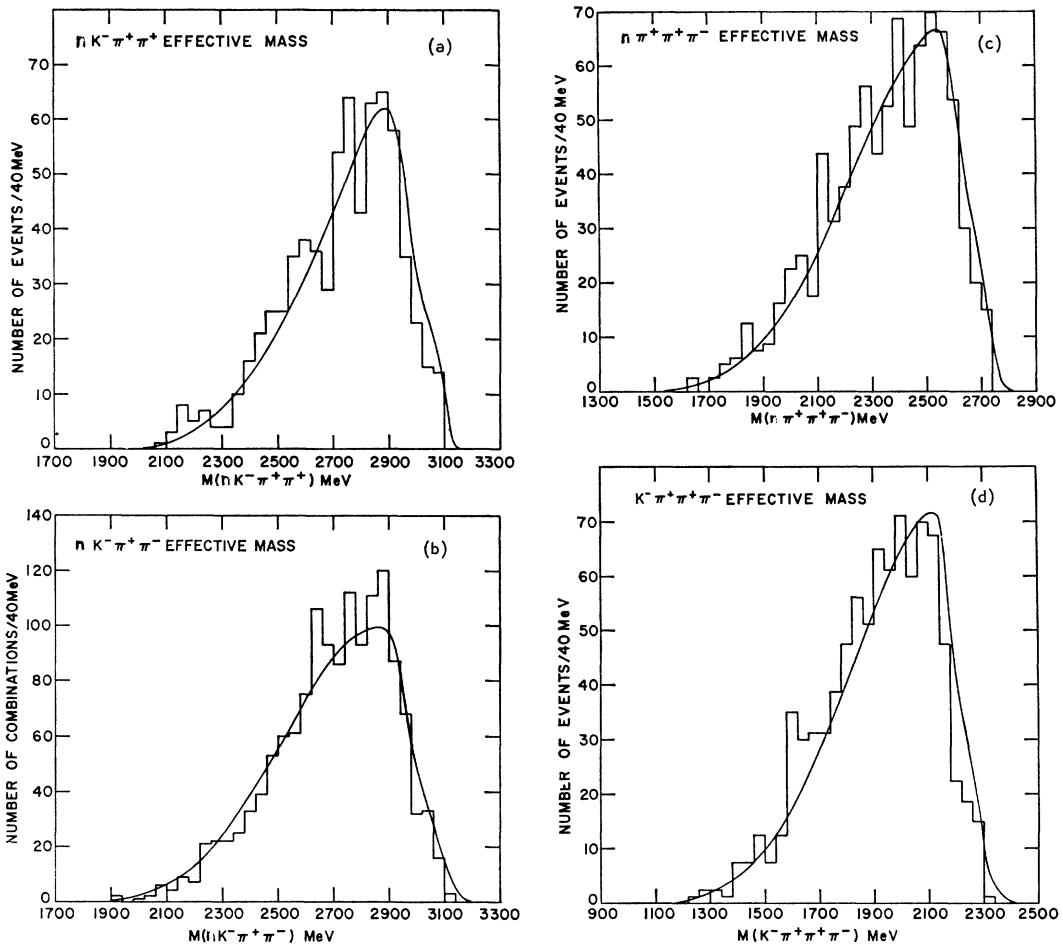

FIG. 20. Four-body mass distributions for reaction (2).

momentum-transfer events with a background correction.

C. 3π Distributions

The gross $\pi^+\pi^+\pi^-$ mass distribution (Fig. 18) exhibits a 4-standard-deviation effect at 960 MeV. This is the same mass at which a 2.5-standard-deviation effect was seen in the $\pi^+\pi^-\pi^0$ distribution for reaction (1). These effects are considered jointly in another paper.[11] The smooth curve in Fig. 18(c) is the result of a maximum-likelihood fit with a Breit-Wigner form for the 960-MeV effect and phase space weighted on the $n\pi^-$ and $K^-\pi^+$ mass distributions. The central peak value of the effect was permitted to vary, but the width was fixed at a value consistent with the calculated mass resolution. The χ^2 probability for a fit using only weighted phase space is 0.12. There is also a weak enhancement in the 1300-MeV mass region of the $\pi^+\pi^+\pi^-$ distribution which may represent a contribution of the A_2^+. However, a fit to this distribution with Breit-Wigner functions for both the 960-MeV effect and the 1300-MeV enhancement yields a zero contribution for this latter effect.

V. $K\pi\pi$ EFFECTS

The *separate* gross $K\pi\pi$ mass distributions for the various combinations which can be formed in reactions (1) and (2) exhibit little clear evidence for either $K_N(1420)$ or $K_A(1320)$. The $K^*(890)\pi$ and $K\rho(760)$ spectra do provide some evidence for these effects, though with limited statistical reliability. In order to achieve a better signal-to-background ratio for these and possibly other $K\pi\pi$ effects with $K^*\pi$ and/or $K\rho$ decays we have *summed* the $K^*(890)\pi$ and $K\rho(760)$ distributions for systems having specific values of I_3. In some instances, two or more mass combinations from the same event are included in a given sample. Interpretation of the resulting distributions requires suitable comparison spectra. For this purpose we use distributions obtained by performing identical operations on phase-space events with the usual weighting included (see Sec. II and Appendix B). No renormal-

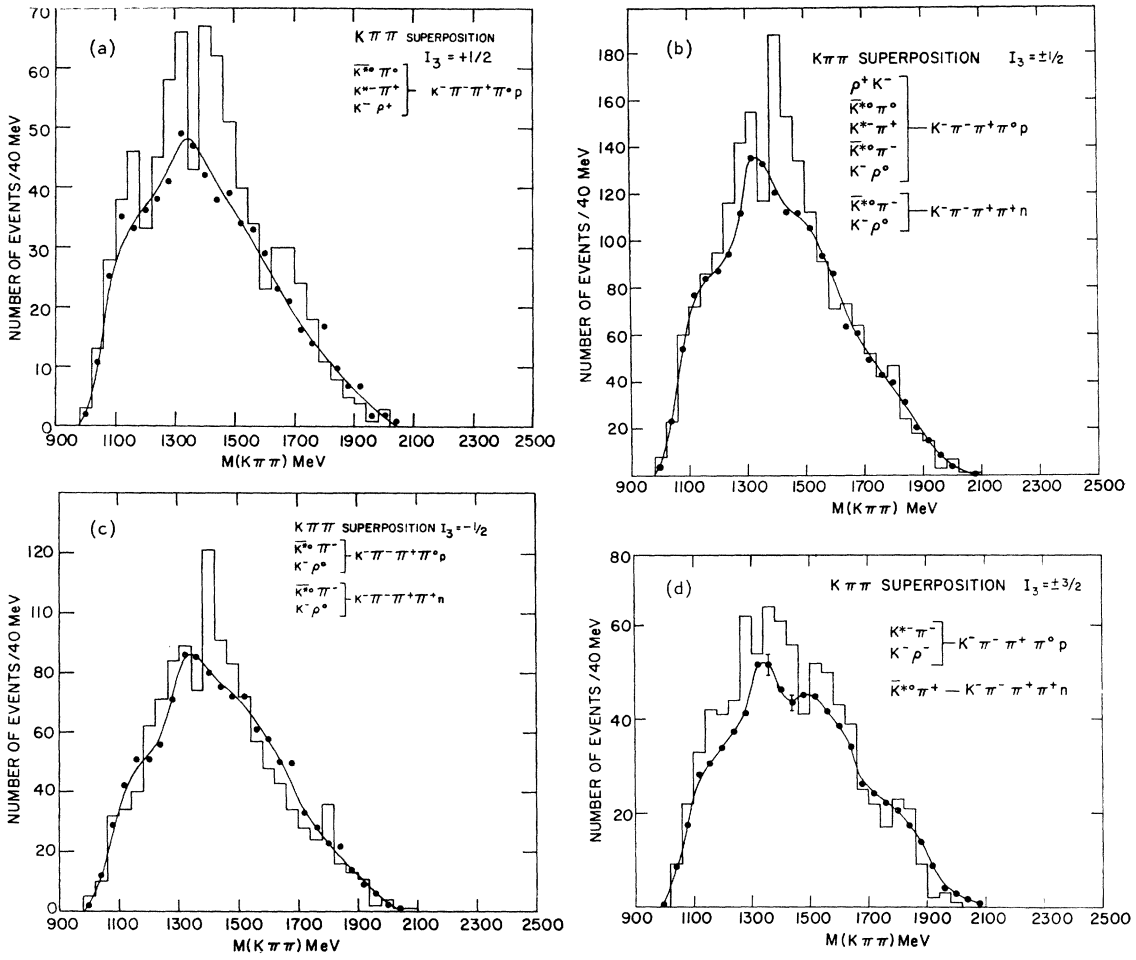

FIG. 21. $K^*\pi$ and $K\rho$ superposed mass distributions from reactions (1) and (2) for $I_3=+\frac{1}{2}$, $I_3=-\frac{1}{2}$, $I_3=\pm\frac{1}{2}$, and $I_3=\pm\frac{3}{2}$ charge states. The various mass combinations contributing to the distributions, and the final state from which they originate, are indicated in the figure. The closed circles indicate the phase-space comparison distribution, which is formed by summing the same selected distributions from samples of Monte-Carlo–generated phase-space events for reactions (1) and (2), with the customary weighting factors included (see Sec. II and Appendix B.).

ization is applied to the curve in this case.[18] Smooth curves are drawn through the weighted-phase-space points, which are indicated in Fig. 21.

The results of this analysis are presented in Fig. 21. The superposition for $I_3=\pm\frac{1}{2}$ and $I_3=\pm\frac{3}{2}$ are also given in Fig. 21. Higher K^*'s (with $K^*\pi$ or $K\rho$ decay modes) produced through exchange of systems with $Q=1$ will contribute to the $I_3=+\frac{1}{2}$ distribution, while those involving $Q=0$ exchange will contribute to the $I_3=-\frac{1}{2}$ spectrum. The distributions for these two charge states differ considerably. While both have strong peaks near 1400 MeV, the $I_3=+\frac{1}{2}$ system also has a strong effect at 1300 MeV, with weaker effects at 1160 and 1660 MeV. The $I_3=-\frac{1}{2}$ system has only an additional weak enhancement at 1300 MeV. Since the $I_3=-\frac{1}{2}$ distribution contains no features which are not also seen in the $I_3=\frac{1}{2}$ spectrum, we conclude that none of the observed effects is produced exclusively by isoscalar exchange. The 1400-MeV effect is of about equal importance in both distributions. This seems also to exclude (for this effect) dominant $I=1$ exchange with an $I=\frac{3}{2}$ recoiling π-nucleon system [taking $I=\frac{1}{2}$ for $K_V(1420)$]. An admixture of these various processes appears more likely. The $I_3=\pm\frac{1}{2}$ superposition yields only two strong effects, the 1300- and 1400-MeV peaks. Other weak effects seen in the $I_3=+\frac{1}{2}$ spectrum are not reinforced here. We conclude that we have evidence in our data for production of $K_A(1320)$ and $K_N(1420)$.

The $I_3=-\frac{3}{2}$ $K\pi\pi$ superpositions involve exchange of $Q=+1$ to the baryon, while the $I_3=+\frac{3}{2}$ distribution (not shown) involves exchange of $Q=-2$. No sta-

[18] The weighted-phase-space comparision curves are expected to be approximately normalized to the background distribution in a given channel (see Appendix B). In the case of the superpositions considered here this approximation appears to work well in that the comparison curves are generally well normalized locally over much of the distribution, deviating principally in the lack of certain additional enhancements which contribute to the experimental data.

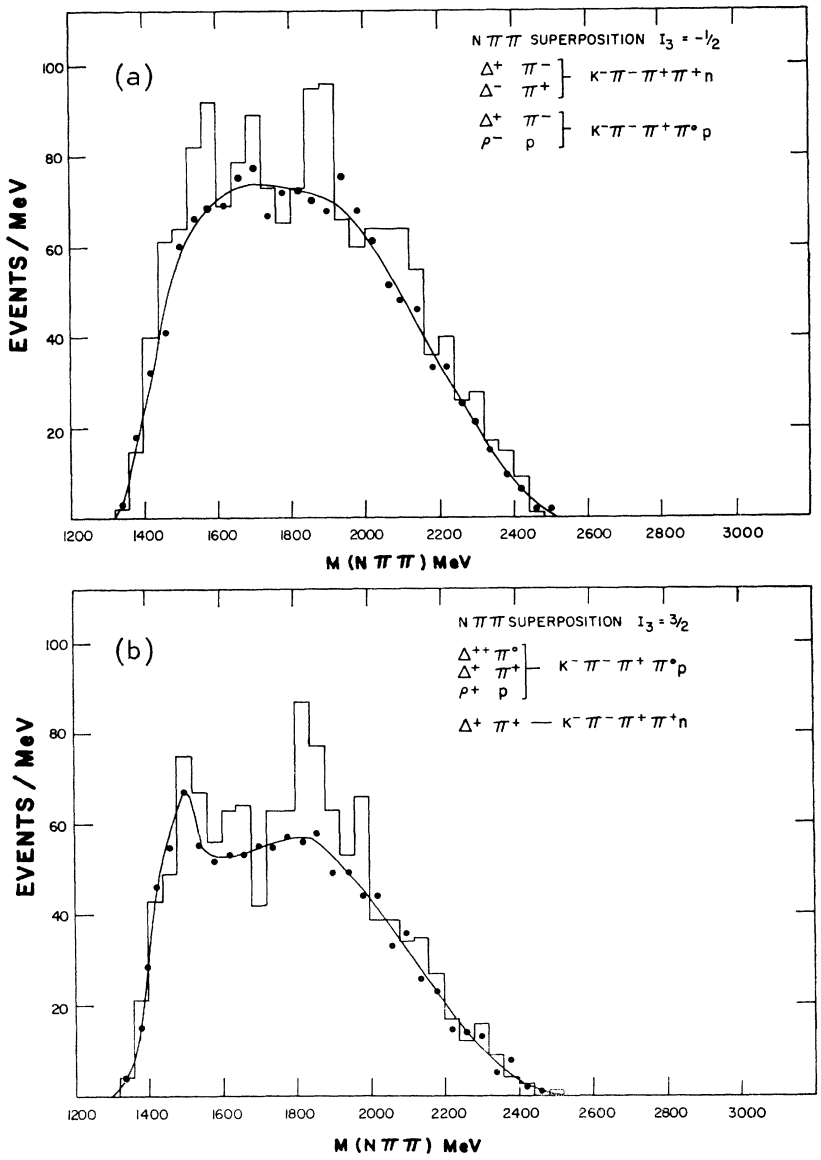

FIG. 22. $\Delta\pi$ and $N\rho$ superposed mass distributions from reactions (1) and (2) for $I_3=-\frac{1}{2}$ and $I_3=\frac{3}{2}$ charge states. These are formed in a manner analogous to the $K^*\pi$ and $K\rho$ distributions of Fig. 21.

tistically significant effects are observed in either the $I_3=-\frac{3}{2}$ or $I_3=\pm\frac{3}{2}$ spectra.

VI. $N\pi\pi$ EFFECTS

In a search for higher N^*'s in our data, we have treated the $N\pi\pi$ distributions in a manner analogous to that previously described for the $K\pi\pi$. Separate superpositions of $\Delta(1236)\pi$ and $\rho(760)N$ distributions for $I_3=\frac{1}{2}$ and $I_3=\frac{3}{2}$ have been formed. These are presented in Fig. 22. Weighted-phase-space curves are shown on the distributions. The $I_3=\frac{3}{2}$ superposition exhibits two peaks, one at 1500 MeV and the other at approximately 1825 MeV. The former peak is probably an artificial peak in the sense that it arises from the summing procedure, since it is well accounted for by the background curve. The 1825-MeV effect, however, is of significance. We have noted effects in this region (Table III) when separately examining the pertinent $I_3=\frac{3}{2}$ $\Delta(1236)\pi$ or ρN distributions. No well-established $I=\frac{3}{2}$ baryon resonance at or near 1825 MeV is known.

The $I_3=\frac{1}{2}$ superposition exhibits effects at 1580, 1700, and 1880 MeV. These could have isotopic spin $\frac{1}{2}$ or $\frac{3}{2}$. The first two are each reasonably consistent in mass and width with one (or more) accepted baryon states, though there is some inconsistency in decay mode. For example, our 1580-MeV effect might be identified with the $N(1570)$ save for the fact that this resonance is reported to have only $N\pi$ and $N\eta$ decay modes.[6] The 1700-MeV peak in our data may be the same effect that is referred to as $N(1688)$.[6] This reso-

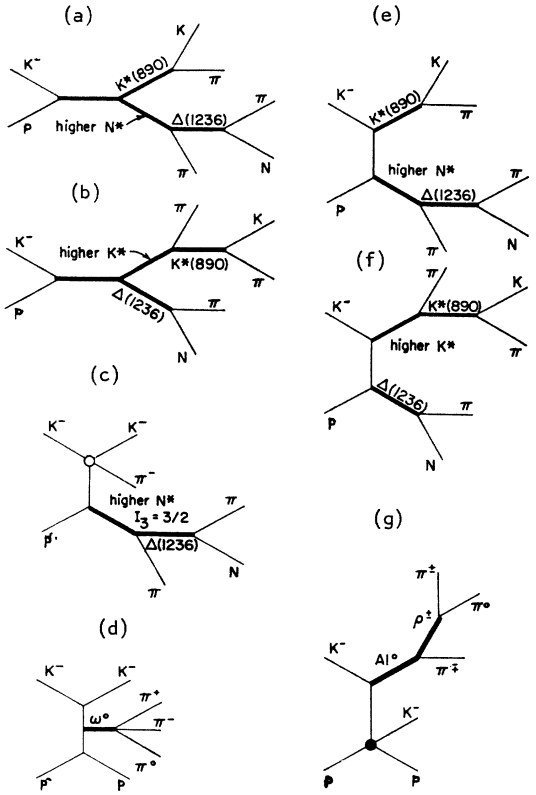

FIG. 23. Diagrams for production processes considered to be contributing to reactions (1) and (2).

nance is reported to have $N\pi\pi$ decay as its dominant inelastic mode; however, the $\Delta(1236)\pi$ branching is reported to be very small. The $I_3=\frac{1}{2}$ 1880-MeV peak is here again not easily identified with known effects. It may be related to the 1820-MeV effect discussed above in connection with our $I_3=\frac{3}{2}$ $N\pi\pi$ superposition. It is possible that some of the effects we see here represent the decays of highly inelastic baryon resonances which have not been identified previously in phase-shift analyses of elastic scattering or in other multiparticle final states.

VII. DISCUSSION AND CONCLUSIONS

The two final states considered in this paper both exhibit strong resonance production. Approximately 80% of the cross section for reaction (1) and 50% for reaction (2) involve effects which can be identified with well-established resonance states. It is possible, as we shall indicate presently, that perhaps even more of the production cross section may involve resonance channels.

We do not observe strong quasi-two-body production in either reaction. Also, simultaneous resonance production in particular channels, e.g., $\bar{K}^{*0}\Delta^{++}(1236)\pi^0$ in reaction (1), is not striking. However, this should not be interpreted to mean that such effects, summed over many possible channels, are not important.

In considering reaction processes contributing to these final states, we refer to Fig. 23. The c.m. forward peaking of the K, $K\pi$, and $K\pi\pi$ systems and the backward peaking of the N, $N\pi$, and $N\pi\pi$ systems indicate that s-channel effects such as those indicated in Figs. 23(a) and 23(b) are not dominant in these reactions. We expect, however, that such processes are probably more important in the five-body states considered here than in two-, three-, or even four-body states produced in K^-p interactions at comparable momenta. The exchange processes indicated in Figs. 23(e) and 23(f) may make a contribution to the cross section for the five-body states considered in this paper. The c.m. angular distributions of the K and baryon systems are qualitatively consistent with this point of view. In this scheme, $\bar{K}^{*0}(890)$, for example, arises in two processes: (1) direct $\bar{K}^{*0}(890)N^*$ production, where N^* refers to some higher N^* with at least an appreciable inelastic decay, and (2) $\Delta(1236)K^*$ production, where K^* refers to a higher K^* resonance such as $K_A(1320)$ or $K_N(1420)$, which has an appreciable $K^*(890)\pi$ decay mode. The higher N^*'s referred to in (1) may have important $\Delta(1236)\pi$ decay branches. Significant contributions from processes such as these do not necessarily require that clearly resolved $K\pi\pi$ or $N\pi\pi$ effects be seen, especially if the density (number of states per unit energy interval) and widths of dominantly inelastic higher K^* or N^* states are large. Actually, however, as indicated in Secs. V and VI, we do have evidence for identifiable $K\pi\pi$ and $N\pi\pi$ states. This picture does imply simultaneous $\Delta(1236)K^*(890)$ production for various charge states. We have noted evidence (Table III) for such effects in this paper.

In Sec. VI we presented evidence for effects near 1825 MeV in the $I_3=+\frac{3}{2}$ $N\pi\pi$ system. Figure 23(c) indicates a suggested production mechanism for this effect involving $K^-\pi^-$ scattering at the upper vertex.

We attribute ω^0 production in these final states largely to the diagram shown in Fig. 23(d). A discussion of possible production mechanisms for the A_1^0 has been presented previously.[13] The general forward preference of the A_1^0 in the c.m. system in conjunction with the strong backward peaking of the proton for A_1^0 events suggests a diagram such as that in Fig. 23(g). Exchange of K^* is possible.

In Ref. 12 we noted that this was the first reported example of A_1^0 production, and also the first case of A_1 production in a reaction in which the conventional Deck effect cannot contribute. More recently, Fridman *et al.*[19] have reported evidence for $A_1^{\pm}$ production in $\bar{p}p$ annihilation ($\bar{p}p\rightarrow 3\pi^+3\pi^-\pi^0$) at 5.7 BeV/$c$. This is, also, a situation in which the Deck effect cannot be

[19] A. Fridman, G. Maurer, A. Michalon, J. Oudet, B. Schiby, R. Strub, C. Voltoline, and P. Cüer, Phys. Rev. **167**, 1268 (1968).

involved. Also, Radlinski *et al.*[20] have reported $A_1^{\pm}$ production in $\bar{p}p \to \pi^+\pi^+\pi^-\pi^-\pi^0$ at 2.4 and 2.9 GeV/c. These results support an interpretation of the A_1 as a "real" resonance, rather than the "kinematic effect" of a particular reaction process, although complications in production and decay processes are not excluded in specific cases. Observation of the A_1^0 appears, also, to exclude an alternative "nonresonant" interpretation of the A_1 given by Gleeson and Meggs,[21] which specifically excludes a neutral A_1 effect.

ACKNOWLEDGMENTS

The authors gratefully acknowledge the assistance of members of the BNL staff in obtaining the exposure on which this paper is based. Thanks are also due to the scanning and measuring staffs of our respective institutions for their important contributions to the processing of the data. The members of the Iowa State group wish, in particular, to thank Professor W. J. Kernan for advice and encouragement throughout the course of the work.

APPENDIX A: BACKGROUND

In Table IV are listed relative background contributions from the principal sources.

The background from "ambiguities with other final states" is estimated from a study of 25% of the $4P1V$ data at 5.0 BeV/c. The most frequent ambiguities are with the states $\pi^+p\pi^-\pi^-\bar{K}^0$, $\pi^+\pi^+\pi^-\pi^-\Lambda^0$, and $\pi^+\pi^+\pi^-\pi^-\Sigma^0$. Since the charged-to-neutral decay rates of the $\bar{K}^0$ and Λ^0 are well known, we are able to determine the number of these final states in which the decay is unseen, and thus estimate the background from them.

The background from the $4C$ state $K^-p\pi^+\pi^-$ is estimated to be less than 1%. Since $4C$ fits for this state are consistent with ionization 95% of the time, the $4C$ fit was always chosen.

The number of fake fits from $\pi^-p\pi^+\pi^-\pi^0$ and $\pi^+n\pi^+\pi^+\pi^-$ states produced by π^- beam contamination is determined from the estimated relative π^- flux in the beam and the relative cross sections for π^-- and K^--induced analog states. In addition, we make the conservative assumption that the kinematic fitting program provides no discrimination between corresponding states initiated by π^- and K^- projectiles.

TABLE IV. Background.

Source	Final state $K^-\pi^-\pi^+\pi^0 p$	Final state $K^-\pi^-\pi^+\pi^+ n$
Ambiguities within the final state (%)	6.5±2.0	2.0±1.0
Fake fits from states having additional missing π^0's (%)	3.0±2.0	1.0±1.0
Ambiguities with other final states (%)	6.0±2.0	14.0±4.0
Fake fits from events produced by the π^- beam contamination (%)	4.0±2.0	4.0±2.0
Total (%)	19.5±4.0	21.0±5.0

[20] R. P. Radlinski, W. J. Kernan, and R. O. Haxby, Bull. Am. Phys. Soc. 14, 181 (1969), Paper AB3; and private communication.
[21] A. M. Gleeson and W. J. Meggs, Syracuse University Report No. SU-1206-139 (unpublished).

APPENDIX B: WEIGHTED PHASE SPACE

Our procedure for correcting the phase-space background in a given channel for resonance effects in other channels can be developed in a formal way in which the assumptions and approximations involved are made explicit. We assume that the differential density distribution in any set of independent invariant masses $m_1 \cdots m_l$ for the final state under consideration can be expressed *approximately* as

$$n_{1\ldots l}(m_1 \cdots m_l) = N\alpha\{\prod_{j=1}^{l}[1+\sum_k C_k{}^j R_k \times (m_j, M_k{}^j, \Gamma_k{}^j)]\}\rho_{1\ldots l}(m_1 \cdots m_l), \quad \text{(B1)}$$

where N is the total number of events, $R_k(m_j, M_k{}^j, \Gamma_k{}^j)$ is a structure form for a resonance k contributing in channel j of central mass $M_k{}^j$ and width $\Gamma_k{}^j$ (we use nonrelativistic Breit-Wigner forms with constant, i.e., mass-independent, widths), $\rho_{1\ldots l}(m_1 \cdots m_l)$ is the invariant phase-space factor, and the $C_k{}^j$ are constants related to the strength of the pure phase-space and kth resonance contributions, respectively, in channel j. We require that $\int dm_j \rho_{1\ldots l}(m_1 \cdots m_l) = 1$. The factor α is a normalization constant. We define

$$\rho_j(m_j) = \int_{i \neq j} dm_i \rho_{1\ldots l}(m_1 \cdots m_l) \quad \text{(B2)}$$

and

$$r_j(m_j) = \alpha_j[1+\textstyle\sum_k C_k{}^j R_k(m_j, M_k{}^j, \Gamma_k{}^j)], \quad \text{(B3)}$$

where α_j is chosen so that

$$\int dm_j r_j(m_j)\rho_j(m_j) = 1. \quad \text{(B4)}$$

We can now write

$$n_{1\ldots l}(m_1 \cdots m_l) = \beta N[\prod_{j=1}^{l} r_j(m_j)]\rho_{1\ldots l}(m_1 \cdots m_l), \quad \text{(B5)}$$

where

$$\beta = \alpha / \prod_{j=1}^{l} \alpha_j.$$

We see here that if $\rho_{1\ldots l}(m_1 \cdots m_l)$ were equal to $\prod_{j=1}^{l} \rho_j(m_j)$, then

$$\alpha = \prod_{j=1}^{l} \alpha_j \quad \text{and} \quad \beta = 1.$$

We note that the parametrization in (B1) implies a series of product-resonance terms which, in a certain sense, correspond to simultaneous resonance effects in

disjoint channels, constructive interference between resonances in intersecting channels, and sequential decays of one resonance into another for adjoint channels. Insofar as such effects are not important in the final state, this feature may be considered a defect in this approach. However, if the individual resonance contributions are fairly small, the product terms are second-order and this objection is less serious. In situations in which simultaneous resonance production in specific disjoint channels dominates, a different parametrization is called for.

The projection in channel i is given as

$$n_i(m_i)=N\beta r_i(m_i)\int_{j\neq i} dm_j[\prod_{j=1}^{l} r_j(m_j)] \times\rho_{1\cdots l}(m_1\cdots m_l) \quad \text{(B6)}$$

or

$$n_i(m_i)=N\beta r_i(m_i)b_i(m_i)\,, \quad \text{(B7)}$$

where $b_i(m_i)$ refers to the integral factor in (B6). If there are no resonances in any but channel i, the $b_i(m_i)$ is the phase-space projection $\rho_i(m_i)$ in channel i, and we have the usual parametrization for a single channel. In order to determine $b_i(m_i)$ we resort to a bootstrap procedure. First, it is assumed that $\beta b_i(m_i)$ is sufficiently similar to $\rho_i(m_i)$ to permit one to estimate $r_i(m_i)$ by the ratio $n_i(m_i)/N\rho_i(m_i)$, i.e., by the ratio of the experimentally observed distribution in channel i to the pure phase-space estimate. Then for the background factor in channel i, $b_i(m_i)$, we use

$$b_i(m_i)=\int_{j\neq i} dm_j \prod_{j=1}^{l}\frac{n_j(m_j)}{N\rho_j(m_j)}\rho_{1\cdots l}(m_1\cdots m_l)\,. \quad \text{(B8)}$$

This integral is performed by Monte Carlo techniques. For each event of a set distributed in m_j according to the invariant phase-space form, we calculate m_i and m_j for all relevant channels. The ratios $n_j(m_j)/\rho_j(m_j)$, referred to as weights, are found from previously prepared tables. We then store in a histogram, in an appropriate bin corresponding to m_i, the product of the various weights. When we use the approximation indicated in (B8), the constant β is very close to 1. This reflects both the suitability of the above-indicated approximations and the extent to which it is valid to replace $\rho_{1\cdots l}(m_1\cdots m_l)$ by a product of projections $\prod_{j=1}^{l}\rho_j(m_j)$.

When weighting on channels for which there are more than one combination per event, e.g., the $K^-\pi^+$ channel in the $K^-n\pi^+\pi^+\pi^-$ final state, the natural extension of this procedure is to use the product of the weights for each of the several combinations, all obtained from the same table.

An important feature of this method is the flexibility it permits for construction of comparison curves for mass projections which are obtained by selecting on or excluding certain mass intervals in other channels. We simply process the phase-space events in the same manner as the real events (indeed, with the same general program), imposing the same kind of cuts, etc., but accumulating weights rather than events.

It is also worth noting here that $N\beta b_i(m_i)$, where again $b_i(m_i)$ is the weighted-phase-space background, is correctly normalized to the background contribution for channel i, at least to the degree that the various approximations permit. However, we have not insisted on this condition in the various applications of weighted phase space and have in certain cases permitted further adjustments required to fit specific distributions.